

# Dynamic Inverse Optimization under Drift and Shocks: Theory, Regret Bounds, and Applications

Jinho Cha<sup>1\*</sup>

<sup>1</sup>\*Department of Computer Science, Gwinnett Technical College,  
Lawrenceville, GA, USA.

Corresponding author(s). E-mail(s): [jcha@GwinnettTech.edu](mailto:jcha@GwinnettTech.edu);

## Abstract

The growing prevalence of drift and shocks in modern decision environments exposes a gap between classical optimization theory and real-world practice. Standard models assume fixed objectives, yet organizations—from hospitals to power grids—routinely adapt to shifting priorities, noisy data, and abrupt disruptions. To address this gap, this study develops a dynamic inverse optimization framework that recovers hidden, time-varying preferences from observed allocation trajectories. The framework unifies identifiability analysis with regret guarantees: conditions are established for existence and uniqueness of recovered parameters, and sharp static and dynamic regret bounds are derived to characterize responsiveness to gradual drift and sudden shocks. Methodologically, a drift-aware estimator grounded in convex analysis and online learning theory is introduced, with finite-sample guarantees on recovery accuracy. Computational experiments in healthcare, energy, logistics, and finance reveal heterogeneous recovery patterns, ranging from rapid resilience to persistent vulnerability. Overall, dynamic inverse optimization emerges as both a theoretical contribution and a broadly applicable diagnostic tool for benchmarking resilience, uncovering hidden behavioral shifts, and guiding policy interventions in complex stochastic systems.

**Keywords:** Inverse Optimization, Dynamic Preferences, Drift and Shocks, Identifiability, Dynamic Regret, Decision Analytics

**Note:** Preprint. Submitted to *Computational Management Science*.

# 1 Introduction

## 1.1 Motivation

Optimization provides the mathematical foundation for decision-making in transportation, energy, finance, and healthcare. Classical approaches assume that objectives such as costs, risks, or fairness weights are known and fixed, and forward optimization then yields optimal allocations. In practice, however, such objectives are rarely transparent. What is typically observable are *decisions themselves*—transport schedules, electricity dispatches, portfolio choices, or triage outcomes—while the implicit trade-offs that generated them remain hidden.

Moreover, these hidden preferences are rarely static. Organizations adapt to fluctuating markets, regulators modify policies, and environments change unexpectedly. As a result, decision-making priorities drift over time. This raises an important question: *Can we recover latent, time-varying preferences from observed allocation trajectories, and evaluate the quality of such recovery?*

## 1.2 Research Gap

Inverse optimization (IO) offers a structured approach to inferring hidden objectives from observed decisions [1, 2]. Applications have appeared in transportation, energy systems, and healthcare [3, 4], and recent surveys highlight its broad methodological scope [5]. At the same time, online convex optimization (OCO) has developed powerful tools for handling non-stationary environments, providing dynamic regret bounds under variation budgets [6–8].

Most existing IO studies remain focused on *static* settings where preferences are fixed, while OCO studies address drift only for forward loss minimization. The intersection—*recovering time-varying latent preferences in applied allocation problems with identifiability and regret guarantees*—has received limited attention. To the best of our knowledge, existing work in online IO has analyzed regret under fixed objectives [9, 10], but the case of drifting objectives within inverse optimization, particularly in applied decision-making contexts, remains relatively unexplored.

## 1.3 Contributions

This paper develops a framework for *dynamic inverse optimization under drift*, linking IO with ideas from OCO and sequential decision analysis. Our contributions are as follows:

1. **Modeling.** We formulate dynamic IO as a bilevel learning problem, where a forward allocation model captures observed behavior and latent preferences evolve subject to bounded variation.
2. **Theoretical Results.** We establish conditions under which identifiability holds, show existence and uniqueness of recovered preference trajectories, and derive static and dynamic regret bounds for drift-aware estimation.

3. **Methodology.** We propose estimation algorithms based on OCO techniques, demonstrating robustness to noise and sample sparsity and the ability to track drifting objectives.
4. **Validation.** Using synthetic yet representative benchmarks (dynamic newsven-dor, multi-period knapsack, interdiction), we illustrate that the proposed approach recovers preference dynamics and achieves consistent performance under uncer-tainty.

By combining identifiability analysis, regret guarantees, and computational validation, the study extends IO beyond static formulations and connects it with dynamic decision contexts. The results contribute to the literature on inverse optimization and sequential decision-making, and suggest the potential of dynamic IO to support applied management science problems where objectives evolve over time.

## 1.4 Paper Structure

The remainder of the paper is organized as follows. Section 3 introduces the forward allocation models and formulates the dynamic IO problem. Section 4 presents theoretical results on identifiability and regret, including the development of estimation algorithms. Section 5 reports computational experiments. Section 6 discusses managerial and industrial implications. Finally, Section 7 concludes with directions for future research.

## 2 Related Literature

### 2.1 Forward Allocation Models

Forward allocation problems remain central in operations research, with recent advances focusing on robustness, fairness, and learning. Robust optimization provides tractable methods for uncertain environments: Ben-Tal and Nemirovski [11] laid the foundations, and Bertsimas and Sim [12] introduced the widely cited concept of the *price of robustness*, quantifying trade-offs between efficiency and worst-case protection. Their ideas quickly spread to applications such as supply chains and energy markets, making robustness a standard design principle.

Fairness has also become integral: Bertsimas, Farias, and Trichakis [13] analyzed the *price of fairness*, and Fournier, Leclere, and Pinson [14] embedded fairness into shared-energy allocation, showing how equity concerns can be built into dynamic stochastic systems. Finally, learning has been incorporated into stochastic settings. Levi, Roundy, and Shmoys [15] and Besbes and Muharremoglu [16] demonstrated how adaptive policies improve allocation under demand uncertainty, highlighting the importance of data-driven and adaptive strategies. Despite these advances, all such models assume that objectives are explicitly specified, rather than inferred from observed decisions.

## 2.2 Inverse Optimization Approaches

Inverse optimization (IO) seeks to recover hidden objective functions from observed decisions. Classic work in operations research established identifiability and consistency properties, with applications in portfolio selection, transportation, and healthcare allocation [1-3]. These foundational contributions demonstrated that IO can serve as a diagnostic tool to reveal implicit trade-offs behind observed behavior, sparking a wide range of applications in data-driven decision contexts.

More recently, emerging research has begun to relax assumptions of stationarity. Inverse optimal control with time-varying cost functions has been explored in human movement analysis, using moving-window techniques to capture changing objectives over the course of a motion [17]. In the control domain, an adaptive online IOC framework using neural networks was introduced, offering real-time estimation of shifting cost weights along with well-posedness and convergence guarantees [18]. From an application standpoint, IO has also been applied to commuter behavior, where [19] recover schedule preferences and crowding perceptions based on aggregate commuting data. These developments signal a growing trend toward dynamic and data-driven IO, highlighting the flexibility of the paradigm across domains ranging from biomechanics to transportation.

However, many existing IO models remain fundamentally *static*, estimating time-invariant objectives from offline data. While some online IO frameworks handle sequential decisions with regret bounds, they still presume a fixed underlying objective and do not address systematic preference drift. Overall, modern studies illustrate the feasibility of dynamic or time-varying IO in specific applications, but a unified framework for drift-aware inverse optimization in resource allocation remains underdeveloped—precisely the gap this paper addresses.

## 2.3 Dynamic Optimization under Drift

In parallel to inverse optimization, online convex optimization (OCO) and non-stationary learning study performance when losses or environments drift over time. The key analytical tools are variation budgets and path length, which quantify cumulative change and enable dynamic regret guarantees. Zinkevich [7] introduced the OCO framework and established regret bounds in sequential convex decision problems. Besbes, Gur, and Zeevi [6] extended this to non-stationary stochastic optimization, deriving sharp lower and upper bounds under variation budgets. Hall and Willett [8] further refined these concepts, applying path-length-based analysis to signal processing and statistical learning tasks, thereby demonstrating the wide applicability of dynamic regret theory.

Subsequent work has broadened scope and refined guarantees. Chiang et al. [20] proposed adaptive variation-based regret bounds that adjust to the degree of non-stationarity, while Mokhtari et al. [21] developed projection-free conditional gradient methods that scale efficiently in high dimensions. Zhang, Chen, and Wang [22] derived tighter guarantees for smooth and strongly convex losses, providing problem-dependent refinements of dynamic regret. More recent studies explore connections to reinforcement learning and distributed optimization, suggesting that dynamic regret

can serve as a unifying principle for adaptation under drift. Collectively, this literature demonstrates how dynamic regret provides rigorous guarantees in changing environments. Yet all of these studies focus on *forward* loss minimization; they do not attempt to recover the hidden, time-varying objectives behind observed decisions. Bridging this gap is the central aim of our work.

## 2.4 Adjacent Areas: IOC/IRL and Applied Mathematics

In control and reinforcement learning, inverse optimal control (IOC) and inverse reinforcement learning (IRL) study the recovery of cost or reward functions from trajectories. Recent extensions allow *time-varying* objectives that adapt weights online and analyze stability or uniqueness in control settings [17, 18]. Neural network-based IOC and IRL methods demonstrate feasibility in robotic and biomechanical systems [23, 24], while non-stationary IRL formulations explicitly account for drifting agent preferences [25]. These approaches emphasize dynamic preference recovery but remain tailored to continuous control or policy learning, with guarantees framed in terms of stability or sample complexity rather than identifiability or regret.

In applied mathematics, *dynamic inverse problems* have been investigated through variational methods. Optimal transport regularization has been used to model time-dependent unknowns as measure-valued curves, ensuring stability of temporal reconstructions [26, 27]. Extensions to imaging and PDE-constrained problems estimate time-varying operators alongside states [28], and generalized conditional gradient algorithms have been proposed for scalable computation with convergence analysis [29]. While mathematically powerful, these works target different forward models than allocation IO and do not provide regret or identifiability results in decision-making contexts.

## 2.5 Positioning Relative to This Work

Across the literature, three themes emerge: (i) inverse optimization largely treats static objectives, with online variants analyzing regret only under fixed preferences; (ii) online convex optimization under drift provides both static and dynamic regret guarantees for forward loss minimization but does not recover latent objectives; and (iii) adjacent areas such as inverse optimal control, inverse reinforcement learning, and applied mathematics explore time variation in other paradigms, but their guarantees focus on stability, sample complexity, or operator recovery rather than identifiability or regret in allocation contexts. The intersection we address—*recovering time-varying latent preferences in allocation models with explicit identifiability conditions and both static and dynamic regret guarantees*—has received only limited systematic attention, and our framework explicitly bridges IO and non-stationary learning while directly targeting preference recovery in allocation settings.

### 3 Model and Problem Formulation

#### 3.1 Forward Allocation Problem

We formalize the forward allocation problem at each period  $t = 1, \dots, T$  as

$$\min_{\mathbf{x} \in \mathcal{X}_t} c_t(\mathbf{x}; \boldsymbol{\theta}_t), \quad (1)$$

where  $\mathcal{X}_t$  denotes the feasible set of allocations and  $c_t(\cdot; \boldsymbol{\theta}_t)$  is the cost function parameterized by a latent preference vector  $\boldsymbol{\theta}_t \in \Theta \subset \mathbb{R}^p$ .

##### 3.1.1 Decision variables and constraints

At each period  $t$ , the decision-maker allocates a resource vector  $\mathbf{x}_t \in \mathbb{R}_+^n$  across a set of  $n$  agents. The feasible set in problem (1) is defined as

$$\mathcal{X}_t := \left\{ \mathbf{x} \in \mathbb{R}_+^n \mid \mathbf{B}_t \mathbf{x} \leq \mathbf{q}_t \right\}, \quad (2)$$

where  $\mathbf{q}_t \in \mathbb{R}_+^k$  represents the available capacity of  $k$  different resources, and  $\mathbf{B}_t \in \mathbb{R}^{k \times n}$  is the resource consumption matrix. Each row of  $\mathbf{B}_t$  corresponds to a specific resource type, each column corresponds to an agent, and the entry  $[\mathbf{B}_t]_{ij}$  indicates how much of resource  $i$  is consumed if agent  $j$  receives one unit of allocation. Thus, the vector  $\mathbf{B}_t \mathbf{x}$  gives the total consumption of each resource across all agents, and the inequality  $\mathbf{B}_t \mathbf{x} \leq \mathbf{q}_t$  ensures that no resource is used beyond its supply.

When  $k = 1$  and  $\mathbf{B}_t = \mathbf{1}^\top$ , the model reduces to the classical single-resource constraint  $\mathbf{1}^\top \mathbf{x} \leq q_t$ . When  $k > 1$ , multiple resource types such as budget, labor, energy, or time can be constrained simultaneously. For example, in a healthcare context,  $\mathbf{q}_t$  may represent the number of ICU and general hospital beds; in logistics, it may capture limits on trucks, drivers, and storage space; and in energy systems, it may reflect available capacities of electricity, gas, and hydrogen. This general form therefore unifies both single-resource and multi-resource allocation problems within a canonical framework.

##### 3.1.2 Cost functions

The objective function in problem (1) is written as

$$c_t : \mathbb{R}^n \times \Theta \rightarrow \mathbb{R}, \quad c_t(\mathbf{x}; \boldsymbol{\theta}_t).$$

Here,  $\boldsymbol{\theta}_t$  encodes the allocator's hidden preferences, trade-off weights, or cost sensitivities. For example, in healthcare allocation  $\boldsymbol{\theta}_t$  may capture priority coefficients across patient groups; in energy systems it may represent environmental regulation weights or risk-aversion parameters; and in education admissions it may reflect the trade-off between academic performance and diversity goals.

**Assumption 1** (Error bound / Polyak–Łojasiewicz (PL) inequality). *For each period  $t = 1, \dots, T$  and parameter vector  $\boldsymbol{\theta}_t \in \Theta$ , the cost function  $c_t$  satisfies the following*

condition [30–35]: there exists a constant  $\mu > 0$  such that

$$\frac{1}{2\mu} \|\nabla_{\mathbf{x}} c_t(\mathbf{x}; \boldsymbol{\theta}_t)\|^2 \geq c_t(\mathbf{x}; \boldsymbol{\theta}_t) - c_t^*(\boldsymbol{\theta}_t), \quad \forall \mathbf{x} \in \mathbb{R}_+^n. \quad (3)$$

where  $c_t^*(\boldsymbol{\theta}_t) = \min_{\mathbf{y} \in \mathcal{X}_t} c_t(\mathbf{y}; \boldsymbol{\theta}_t)$ .

The PL inequality lies between convexity and strong convexity [35]. It provides a quantitative link between the optimality gap, the norm of the gradient, and the distance to the solution. While direct verification of PL conditions can be challenging, many allocation-type cost functions such as quadratic congestion costs, regularized fairness penalties, or log-barrier utilities are known to satisfy this property [33, 34]. Moreover, recent results show that PL-type conditions can hold even for some nonconvex structures [30, 31, 36], making it a practical and broadly applicable assumption. This regularity condition relaxes strong convexity while still ensuring stability of solutions and linear convergence of first-order methods, and it plays a central role in establishing identifiability of the parameters, uniqueness of the forward problem solution, and regret guarantees in the dynamic inverse optimization framework developed in subsequent sections.

### 3.2 Inverse Problem Definition

The forward allocation model describes how a decision-maker selects  $\mathbf{x}_t$  given hidden parameters  $\boldsymbol{\theta}_t$ . In practice, however, the analyst does not observe  $\boldsymbol{\theta}_t$  directly. Instead, only the allocation decisions  $\mathbf{x}_t$  and the problem data  $(\mathbf{B}_t, \mathbf{q}_t)$  are observed. The inverse problem is therefore to recover  $\boldsymbol{\theta}_t$  from these observations under suitable regularity conditions.

#### 3.2.1 Loss functions

To evaluate how well a candidate parameter vector  $\boldsymbol{\theta} \in \Theta$  explains the observed allocation  $\mathbf{x}_t$ , we construct a loss function based on the violation of the optimality system associated with problem (1). Specifically, consider the Karush–Kuhn–Tucker (KKT) conditions at time  $t$ : (i) primal feasibility,  $\mathbf{B}_t \mathbf{x}_t \leq \mathbf{q}_t$ ; (ii) dual feasibility,  $\boldsymbol{\lambda}_t \geq \mathbf{0}$ ; and (iii) complementary slackness,  $\boldsymbol{\lambda}_t^\top (\mathbf{B}_t \mathbf{x}_t - \mathbf{q}_t) = 0$ . Here,  $\nabla_{\mathbf{x}} c_t(\mathbf{x}_t; \boldsymbol{\theta})$  denotes the gradient of the cost function, and  $\boldsymbol{\lambda}_t \in \mathbb{R}_+^k$  are the Lagrange multipliers. The optimality system requires that

$$\nabla_{\mathbf{x}} c_t(\mathbf{x}_t; \boldsymbol{\theta}) + \mathbf{B}_t^\top \boldsymbol{\lambda}_t = \mathbf{0}, \quad \boldsymbol{\lambda}_t \geq \mathbf{0}, \quad \mathbf{B}_t \mathbf{x}_t \leq \mathbf{q}_t, \quad \boldsymbol{\lambda}_t^\top (\mathbf{B}_t \mathbf{x}_t - \mathbf{q}_t) = 0. \quad (4)$$

**Assumption 2** (KKT regularity). *For each  $t$ , the observed allocation  $\mathbf{x}_t$  together with the problem data  $(\mathbf{B}_t, \mathbf{q}_t)$  admits some latent parameter  $\boldsymbol{\theta}_t \in \Theta$  and multipliers  $\boldsymbol{\lambda}_t \in \mathbb{R}_+^k$  such that the KKT system (4) holds exactly.*

Given observed  $\mathbf{x}_t$ , these conditions may not hold exactly for an arbitrary  $\boldsymbol{\theta}$ . We therefore define the loss at time  $t$  as the magnitude of violation:

$$\ell_t(\boldsymbol{\theta}) := \underbrace{\|(\mathbf{B}_t \mathbf{x}_t - \mathbf{q}_t)_+\|^2}_{\text{primal feasibility gap}} + \underbrace{\inf_{\boldsymbol{\lambda}_t \geq \mathbf{0}} \|\nabla_{\mathbf{x}} c_t(\mathbf{x}_t; \boldsymbol{\theta}) + \mathbf{B}_t^\top \boldsymbol{\lambda}_t\|^2}_{\text{dual feasibility gap}} + \underbrace{|\boldsymbol{\lambda}_t^\top (\mathbf{B}_t \mathbf{x}_t - \mathbf{q}_t)|}_{\text{complementarity gap}}. \quad (5)$$

This generalized optimality-gap loss jointly penalizes violations of primal feasibility, dual feasibility, and complementarity. Importantly, Assumptions 1 and 2 ensure that this loss is not merely heuristic but theoretically grounded: the PL inequality guarantees that small violations of the optimality system imply a small optimality gap, while KKT regularity ensures that observed allocations are consistent with some true parameter vector. Thus, the error bound property rigorously links allocation discrepancies to the forward problem's solution quality, providing a solid foundation for inverse estimation.

### 3.2.2 Objective of parameter recovery

Aggregating over  $T$  periods, the inverse optimization estimator is defined as

$$\hat{\boldsymbol{\theta}} \in \arg \min_{\boldsymbol{\theta} \in \Theta} \sum_{t=1}^T \ell_t(\boldsymbol{\theta}). \quad (6)$$

This formulation directly ties parameter recovery to observed allocation data. By minimizing the cumulative violation of the KKT system, the estimator  $\hat{\boldsymbol{\theta}}$  recovers the latent preferences or trade-offs that best rationalize the decision-maker's observed choices. Together with Assumption 1, this framework establishes consistency between the forward model and the inverse estimator, and it sets the stage for the identifiability and regret analysis developed in the next section.

## 3.3 Dynamic Drift

### 3.3.1 Variation budget

To capture temporal nonstationarity, we define the *variation budget*

$$V_T := \sum_{t=2}^T d(\boldsymbol{\theta}_t, \boldsymbol{\theta}_{t-1}), \quad (7)$$

where  $d(\cdot, \cdot)$  is a metric on  $\Theta$ , which may be taken as the Euclidean norm, the  $\ell_1$  norm, a Wasserstein distance, or more generally a Bregman divergence. This general formulation allows us to analyze a wide class of nonstationary environments.

We assume that  $V_T$  is bounded in growth relative to the horizon length:

$$V_T = O(T^\alpha), \quad \alpha < 1.$$

This condition, standard in dynamic regret analysis [37, 38], implies that the cumulative drift grows sublinearly with time, so the environment evolves but does not change arbitrarily fast. When  $V_T = 0$ , the setting reduces to the stationary case. When  $V_T$  is small but positive, the environment exhibits gradual drift; large but infrequent changes can be modeled as jump shocks, which we separate from smooth drift by writing  $V_T = V_T^{\text{smooth}} + V_T^{\text{shock}}$ .

### 3.3.2 Behavioral interpretation

The variation budget  $V_T$  can be interpreted as a “budget of change” in the decision-maker’s latent preferences. For example, in energy allocation,  $\theta_t$  may shift due to sudden regulatory interventions (jump shocks) combined with gradual shifts in sustainability priorities (smooth drift). In healthcare,  $\theta_t$  may undergo abrupt changes at the onset of a pandemic followed by gradual adaptation to evolving patient demand. In logistics and supply chains,  $V_T$  may capture seasonal fluctuations with predictable smooth variation, interrupted by occasional shocks such as strikes or supply disruptions. This decomposition emphasizes that the variation budget is not only a mathematical device but also an interpretable measure of how preferences evolve in realistic dynamic environments.

## 4 Theoretical Results

Before presenting detailed results, we briefly group the assumptions used throughout this section. *Structural assumptions* concern the geometry of the forward model (Polyak–Łojasiewicz inequality, KKT regularity, and projected-gradient injectivity). *Regularity assumptions* ensure well-posedness (level-boundedness, compactness, and quadratic growth). *Statistical assumptions* capture data properties (bounded subgradients, drift conditions, and noise models). This classification helps clarify which results rely on structural identifiability, which on optimization regularity, and which on stochastic robustness.

Table 1 summarizes the main notation used in the theoretical analysis. We group symbols into decision variables, model parameters, operators, and statistical quantities to facilitate readability and avoid ambiguity in later results.

### 4.1 Identifiability

We first establish conditions under which the latent preference parameters  $\theta_t$  are uniquely identifiable from observed allocation data. Throughout, we rely on *structural assumptions* introduced in Section 4, namely the PL condition, KKT regularity, and projected-gradient injectivity.

**Table 1** Summary of notation used in the theoretical analysis

Symbol	Description
<b>Decision variables</b>	
$\mathbf{x}_t \in \mathbb{R}_+^n$	Allocation decision vector at period $t$
$\hat{\theta}_t$	Estimated parameter at period $t$
<b>Parameters</b>	
$\theta_t \in \Theta \subset \mathbb{R}^p$	Latent preference parameter at period $t$
$c_t(\mathbf{x}; \theta)$	Cost function at period $t$
$\mathbf{B}_t \in \mathbb{R}^{k \times n}$	Constraint matrix at period $t$
$\mathbf{q}_t \in \mathbb{R}^k$	Capacity/right-hand side vector at period $t$
$\mathbf{A}_t(\mathbf{x}) \in \mathbb{R}^{n \times p}$	Jacobian matrix of $\nabla_{\mathbf{x}} c_t(\mathbf{x}; \theta)$ wrt $\theta$
$\mathbf{b}_t(\mathbf{x}) \in \mathbb{R}^n$	Offset vector in linear gradient representation
$\Theta$	Feasible parameter set
<b>Dual variables</b>	
$\lambda_t \in \mathbb{R}_+^k$	Lagrange multipliers at period $t$
<b>Operators and functions</b>	
$\ell_t(\theta)$	Inverse loss at period $t$
$P_t$	Orthogonal projector onto $\ker(\mathbf{B}_t)$
$\mathbf{I}$	Identity matrix
$\mathbf{1}$	All-ones vector
$\Pi_{\mathcal{K}}(\mathbf{v})$	Projection of $\mathbf{v}$ onto convex cone $\mathcal{K}$
$d(\cdot, \cdot)$	Metric/divergence on $\Theta$
$\langle \mathbf{u}, \mathbf{v} \rangle$	Euclidean inner product $\mathbf{u}^\top \mathbf{v}$
$\ \mathbf{u}\ $	Euclidean norm of vector $\mathbf{u}$
<b>Statistical/structural quantities</b>	
$V_T$	Variation budget $\sum_{t=2}^T \ \theta_t - \theta_{t-1}\ $
$\mu$	PL inequality constant
$\sigma^2$	Variance proxy of sub-Gaussian noise
$\kappa$	Strong identifiability modulus
$G$	Uniform subgradient bound

### Preliminaries.

$\mathbf{A}^\dagger$ : Moore–Penrose pseudoinverse.  $\text{range}(\mathbf{A})$ ,  $\ker(\mathbf{A})$ : range and nullspace.  $\Pi_{\mathcal{K}}(\mathbf{v})$ : Euclidean projection of  $\mathbf{v}$  onto a closed convex cone  $\mathcal{K}$ ; single-valued, nonexpansive, and  $\mathbf{v} - \Pi_{\mathcal{K}}(\mathbf{v})$  orthogonal to  $\mathcal{K}$ .  $\langle \mathbf{u}, \mathbf{v} \rangle = \mathbf{u}^\top \mathbf{v}$ ,  $\|\mathbf{u}\|$ : Euclidean norm.

**Lemma 1** (Projector properties). *Let  $\mathbf{B}_t \in \mathbb{R}^{k \times n}$  and define*

$$P_t := I - \mathbf{B}_t^\top (\mathbf{B}_t \mathbf{B}_t^\top)^\dagger \mathbf{B}_t \in \mathbb{R}^{n \times n}. \quad (8)$$

*Then  $P_t$  is (i) symmetric, (ii) idempotent, and (iii)  $P_t \mathbf{B}_t^\top = 0$ . In particular,  $P_t$  is the orthogonal projector onto  $\ker(\mathbf{B}_t)$  along  $\text{range}(\mathbf{B}_t^\top)$ .*

*Proof (i) Symmetry.* Since  $\mathbf{B}_t \mathbf{B}_t^\top$  is symmetric positive semidefinite, its Moore–Penrose pseudoinverse  $(\mathbf{B}_t \mathbf{B}_t^\top)^\dagger$  is symmetric. Thus

$$P_t^\top = I - \mathbf{B}_t^\top ((\mathbf{B}_t \mathbf{B}_t^\top)^\dagger)^\top \mathbf{B}_t = I - \mathbf{B}_t^\top (\mathbf{B}_t \mathbf{B}_t^\top)^\dagger \mathbf{B}_t = P_t.$$

Table 2 Dependency of assumptions across main theoretical results, grouped by subsection

Assumption	Lemma 1	Lemma 2	Lemma 3	Lemma 4	Lemma 5	Lemma 6	Prop. 1	Cor. 1	Cor. 2	Thm. 3	Thm. 4	Thm. 5	Thm. 6	Notes
<b>Identifiability (Section 4.1)</b>														
Assump. 1 (PL inequality)	✓	✓	✓	✓	✓	✓	✓	✓	✓	✓	✓	✓	✓	Identifiability, Regret, Noise
Assump. 2 (KKT regularity)	✓	✓	✓	✓	✓	✓	✓	✓	✓	✓	✓	✓	✓	Structural feasibility assumption
Assump. 3 (Injectivity)	✓	✓	✓	✓	✓	✓	✓	✓	✓	✓	✓	✓	✓	Identifiability, Noise
<b>Existence and Uniqueness (Section 4.2)</b>														
Assump. 4 (Level-boundedness / Compactness)					✓									Existence
Assump. 5 (Quadratic growth)					✓									Existence
Assump. 6 (Continuity + Compactness for inverse loss)					✓									Existence
<b>Static and Dynamic Regret (Section 4.3)</b>														
Assump. 7 (Uniform subgradients)							✓	✓						Regret
Assump. 8 (Drift sq-summability)							✓	✓						Regret
<b>Noise Robustness (Section 4.4)</b>														
Assump. 9 (Noise smoothness + Strong identifiability)										✓				Noise Robustness

(ii) *Idempotence*. Expanding gives

$$P_t^2 = I - 2\mathbf{B}_t^\top (\mathbf{B}_t \mathbf{B}_t^\top)^\dagger \mathbf{B}_t + \mathbf{B}_t^\top (\mathbf{B}_t \mathbf{B}_t^\top)^\dagger (\mathbf{B}_t \mathbf{B}_t^\top) (\mathbf{B}_t \mathbf{B}_t^\top)^\dagger \mathbf{B}_t.$$

The defining property of the pseudoinverse ensures  $(\mathbf{B}_t \mathbf{B}_t^\top)^\dagger (\mathbf{B}_t \mathbf{B}_t^\top) (\mathbf{B}_t \mathbf{B}_t^\top)^\dagger = (\mathbf{B}_t \mathbf{B}_t^\top)^\dagger$ . Substituting, the last term reduces to  $\mathbf{B}_t^\top (\mathbf{B}_t \mathbf{B}_t^\top)^\dagger \mathbf{B}_t$ , so  $P_t^2 = P_t$ .

(iii) *Annihilation of  $\mathbf{B}_t^\top$* . We compute

$$P_t \mathbf{B}_t^\top = \mathbf{B}_t^\top - \mathbf{B}_t^\top (\mathbf{B}_t \mathbf{B}_t^\top)^\dagger \mathbf{B}_t \mathbf{B}_t^\top.$$

Now  $(\mathbf{B}_t \mathbf{B}_t^\top)^\dagger (\mathbf{B}_t \mathbf{B}_t^\top)$  is the orthogonal projector onto  $\text{range}(\mathbf{B}_t)$ , so the product equals  $\mathbf{B}_t^\top$ . Hence  $P_t \mathbf{B}_t^\top = 0$ .

Combining (i)–(iii),  $P_t$  is a symmetric idempotent matrix annihilating  $\text{range}(\mathbf{B}_t^\top)$ , which by definition is the orthogonal projector onto  $\ker(\mathbf{B}_t)$  along  $\text{range}(\mathbf{B}_t^\top)$ .  $\square$

**Lemma 2** (KKT consistency from zero loss). *Fix  $t$  and suppose Assumptions 1 (Structural) hold. Recall the generalized inverse loss  $\ell_t(\boldsymbol{\theta})$  defined in (5). Then  $\ell_t(\boldsymbol{\theta}) = 0$  if and only if there exists  $\boldsymbol{\lambda}_t(\boldsymbol{\theta}) \geq 0$  satisfying the KKT system (4).*

*Proof* ( $\Rightarrow$ ) Suppose  $\ell_t(\boldsymbol{\theta}) = 0$ . By definition of the loss (5), the primal feasibility gap, dual feasibility gap, and complementarity gap must all vanish. Hence there exists  $\boldsymbol{\lambda}_t(\boldsymbol{\theta}) \geq 0$  such that

$$\nabla_{\mathbf{x}} c_t(\mathbf{x}_t; \boldsymbol{\theta}) + \mathbf{B}_t^\top \boldsymbol{\lambda}_t(\boldsymbol{\theta}) = 0, \quad \mathbf{B}_t \mathbf{x}_t \leq \mathbf{q}_t, \quad \boldsymbol{\lambda}_t(\boldsymbol{\theta})^\top (\mathbf{B}_t \mathbf{x}_t - \mathbf{q}_t) = 0,$$

which is exactly the KKT system.

( $\Leftarrow$ ) Conversely, if there exists  $\boldsymbol{\lambda}_t(\boldsymbol{\theta}) \geq 0$  such that the KKT system holds, then all three gaps are zero by construction. Thus  $\ell_t(\boldsymbol{\theta}) = 0$ .  $\square$

**Lemma 3** (Zero loss implies projected-gradient consistency). *Under Assumptions 1 and 2, if  $\ell_t(\boldsymbol{\theta}) = 0$  then*

$$P_t \nabla_{\mathbf{x}} c_t(\mathbf{x}_t; \boldsymbol{\theta}) = 0, \quad P_t \nabla_{\mathbf{x}} c_t(\mathbf{x}_t; \boldsymbol{\theta}_t) = 0.$$

*Proof* If  $\ell_t(\boldsymbol{\theta}) = 0$ , then by Lemma 2 there exists  $\boldsymbol{\lambda}_t(\boldsymbol{\theta}) \geq 0$  such that

$$\nabla_{\mathbf{x}} c_t(\mathbf{x}_t; \boldsymbol{\theta}) + \mathbf{B}_t^\top \boldsymbol{\lambda}_t(\boldsymbol{\theta}) = 0.$$

Multiplying both sides by  $P_t$  and using  $P_t \mathbf{B}_t^\top = 0$  from Lemma 1 gives

$$P_t \nabla_{\mathbf{x}} c_t(\mathbf{x}_t; \boldsymbol{\theta}) = 0.$$

An identical argument applied with the true parameter  $\boldsymbol{\theta}_t$  shows

$$P_t \nabla_{\mathbf{x}} c_t(\mathbf{x}_t; \boldsymbol{\theta}_t) = 0.$$

$\square$

**Assumption 3** (Projected gradient injectivity (Structural)). *For each  $t$ , the mapping  $\boldsymbol{\theta} \mapsto P_t \nabla_{\mathbf{x}} c_t(\mathbf{x}_t; \boldsymbol{\theta})$  is injective on  $\Theta$ .*

**Theorem 1** (Pointwise identifiability) *Suppose Assumptions 1, 2, and 3 hold, and  $\mathbf{x}_t$  is observed without noise. Then*

$$\ell_t(\boldsymbol{\theta}) = 0 \implies \boldsymbol{\theta} = \boldsymbol{\theta}_t.$$

Thus, exact fit of the inverse loss uniquely recovers the true parameter at time  $t$ .

*Proof* Suppose  $\ell_t(\boldsymbol{\theta}) = 0$ . By Lemma 2, this implies that the KKT system (4) is satisfied at  $(\mathbf{x}_t, \boldsymbol{\theta})$ . Under Assumptions 1, 2, and 3, the KKT system uniquely identifies the latent parameter  $\boldsymbol{\theta}_t$ . Hence  $\boldsymbol{\theta} = \boldsymbol{\theta}_t$ .

Conversely, if  $\boldsymbol{\theta} = \boldsymbol{\theta}_t$ , then  $\mathbf{x}_t$  is by definition the optimizer of the forward problem under  $\boldsymbol{\theta}_t$ , so the KKT system holds exactly. Thus  $\ell_t(\boldsymbol{\theta}_t) = 0$ .  $\square$

**Corollary 1** (Global identifiability under stationarity). *If  $\boldsymbol{\theta}_t \equiv \boldsymbol{\theta}$  for all  $t$ , then*

$$\sum_{t=1}^T \ell_t(\boldsymbol{\theta}') = 0 \implies \boldsymbol{\theta}' = \boldsymbol{\theta}.$$

Hence, stationarity across time implies global recovery of the common parameter.

*Proof* Suppose  $\boldsymbol{\theta}_t \equiv \boldsymbol{\theta}$  for all  $t$ . If  $\sum_{t=1}^T \ell_t(\boldsymbol{\theta}') = 0$ , then each summand satisfies  $\ell_t(\boldsymbol{\theta}') = 0$ . By Theorem 1, this implies  $\boldsymbol{\theta}' = \boldsymbol{\theta}_t = \boldsymbol{\theta}$  for every  $t$ . Hence  $\boldsymbol{\theta}' = \boldsymbol{\theta}$ , establishing global identifiability.  $\square$

**Proposition 1** (Consistency across time implies stationarity) *If there exists  $\bar{\boldsymbol{\theta}}$  such that  $\ell_t(\bar{\boldsymbol{\theta}}) = 0$  for all  $t$ , then necessarily  $\boldsymbol{\theta}_t \equiv \bar{\boldsymbol{\theta}}$ .*

*Proof* Suppose there exists  $\bar{\boldsymbol{\theta}}$  such that  $\ell_t(\bar{\boldsymbol{\theta}}) = 0$  for all  $t$ . Then, by Theorem 1,  $\bar{\boldsymbol{\theta}} = \boldsymbol{\theta}_t$  for each  $t$ . Therefore all  $\boldsymbol{\theta}_t$  must be equal to the same  $\bar{\boldsymbol{\theta}}$ , i.e.  $\boldsymbol{\theta}_t \equiv \bar{\boldsymbol{\theta}}$ . This shows that temporal consistency of the inverse loss implies parameter stationarity.  $\square$

#### Linear-in-parameter specialization.

Assume  $\nabla_{\mathbf{x}} c_t(\mathbf{x}; \boldsymbol{\theta}) = \mathbf{A}_t(\mathbf{x})\boldsymbol{\theta} + \mathbf{b}_t(\mathbf{x})$ . Define  $\tilde{\mathbf{A}}_t := \mathbf{P}_t \mathbf{A}_t(\mathbf{x}_t)$  and  $\mathcal{A} := [\tilde{\mathbf{A}}_1; \dots; \tilde{\mathbf{A}}_T]$ .

**Theorem 2** (Identifiability under linear structure) 1. *If  $\text{rank}(\tilde{\mathbf{A}}_t) = p$  for some  $t$ , then  $\ell_t(\boldsymbol{\theta}) = 0 \Rightarrow \boldsymbol{\theta} = \boldsymbol{\theta}_t$ .*  
2. *If  $\boldsymbol{\theta}_t \equiv \boldsymbol{\theta}$  and  $\text{rank}(\mathcal{A}) = p$ , then  $\sum_t \ell_t(\boldsymbol{\theta}') = 0 \Rightarrow \boldsymbol{\theta}' = \boldsymbol{\theta}$ .*

**Corollary 2** (Rank conditions and modulus). *Identifiability reduces to full column rank of  $\tilde{\mathbf{A}}_t$  (pointwise) or  $\mathcal{A}$  (stationary). The identifiability modulus is lower bounded by the squared smallest singular value, providing stability guarantees.*

*Proof* Part (1) of Theorem 2 shows that pointwise identifiability holds if  $\tilde{\mathbf{A}}_t$  has full column rank. Part (2) shows that stationary identifiability holds if  $\mathcal{A}$  has full column rank. Hence identifiability is equivalent to these rank conditions.

Furthermore, stability follows from perturbation analysis: for any  $\Delta\boldsymbol{\theta}$ ,

$$\|\mathcal{A}\Delta\boldsymbol{\theta}\|^2 \geq \sigma_{\min}^2(\mathcal{A}) \|\Delta\boldsymbol{\theta}\|^2,$$

where  $\sigma_{\min}(\mathcal{A})$  is the smallest singular value of  $\mathcal{A}$ . Thus the identifiability modulus  $\kappa$  is lower bounded by  $\sigma_{\min}^2(\mathcal{A})$ , ensuring robustness of recovery under noise and approximation error.  $\square$

If  $c_t(\cdot; \boldsymbol{\theta})$  is scale-invariant, identifiability holds only up to scaling; a normalization (e.g.,  $\|\boldsymbol{\theta}\|_2 = 1$ ) is imposed in such cases.

## 4.2 Existence and Uniqueness

We next establish well-posedness of both the forward allocation problem and the inverse estimator. *Existence* ensures that a feasible solution to each problem always exists, while *uniqueness* ensures that the solution and recovered parameter are not ambiguous. These results rely primarily on the *regularity assumptions*.

**Assumption 4** (Level-boundedness / coercivity or compactness (Regularity)). *For each  $t$ , either  $X_t$  is compact, or  $c_t(\cdot; \boldsymbol{\theta}_t)$  is level-bounded (coercive) over  $X_t$  so that  $\{\mathbf{x} \in X_t : c_t(\mathbf{x}; \boldsymbol{\theta}_t) \leq \alpha\}$  is compact for all  $\alpha$ .*

**Assumption 5** (Quadratic growth (Regularity)). *For each  $t$ ,  $c_t(\cdot; \boldsymbol{\theta}_t)$  is convex on  $X_t$  and satisfies a quadratic growth condition: there exists  $\alpha_t > 0$  such that*

$$c_t(\mathbf{x}; \boldsymbol{\theta}_t) - c_t(\mathbf{x}_t^*; \boldsymbol{\theta}_t) \geq \frac{\alpha_t}{2} \|\mathbf{x} - \mathbf{x}_t^*\|^2, \quad \forall \mathbf{x} \in X_t.$$

**Assumption 6** (Continuity and compactness for inverse loss (Regularity)). *Each  $\ell_t(\boldsymbol{\theta})$  is lower semicontinuous in  $\boldsymbol{\theta}$ , and  $\Theta$  is compact (or  $\sum_{t=1}^T \ell_t(\boldsymbol{\theta})$  is coercive on  $\Theta$ ).*

**Theorem 3** (Existence and Uniqueness of Solutions) *Suppose Assumptions 2, 4, and 5 hold. Then:*

1. **Forward problem.** For each  $t = 1, \dots, T$ , the allocation problem

$$\min_{\mathbf{x} \in X_t} c_t(\mathbf{x}; \boldsymbol{\theta}_t) \tag{9}$$

*admits at least one solution, and the solution  $\mathbf{x}_t^*$  is unique.*

2. **Inverse estimator.** If, in addition, Assumption 6 holds, then the inverse estimator

$$\hat{\boldsymbol{\theta}} \in \arg \min_{\boldsymbol{\theta} \in \Theta} \sum_{t=1}^T \ell_t(\boldsymbol{\theta}) \tag{10}$$

*admits at least one minimizer. Furthermore, under identifiability (Assumption 3) with noiseless observations, the minimizer is unique and coincides with the true parameter.*

*Proof (i) Forward:* By Assumption 2,  $X_t$  is nonempty, convex, and closed. Assumption 4 yields existence of a minimizer via Weierstrass. Uniqueness follows from Assumption 5, since otherwise two distinct minimizers would contradict quadratic growth.

*(ii) Inverse:* Lower semicontinuity of  $\ell_t$  and compactness (or coercivity) in  $\boldsymbol{\theta}$  ensure existence of a minimizer of (10). In the noiseless setting,  $\ell_t(\boldsymbol{\theta}_t) = 0$  and, by Assumption 3 (or

Theorem 2),  $\sum_{t=1}^T \ell_t(\boldsymbol{\theta}) = 0$  implies  $\boldsymbol{\theta} = \boldsymbol{\theta}_t$ . Hence the minimizer is unique and matches the true parameter.  $\square$

Together, these results establish that both the forward allocation problem and the inverse estimation problem are *well-posed*: solutions always exist and are unique under the stated structural and regularity assumptions.

### 4.3 Static and Dynamic Regret

We now analyze the performance of the inverse optimization estimator in terms of regret. *Static regret* measures error relative to the best fixed comparator parameter, while *dynamic regret* accounts for temporal variation in the true parameter sequence. These guarantees rely on *statistical assumptions*: bounded subgradients (Assumption 7) and square-summable drift (Assumption 8). This separation clarifies that structural identifiability (Section 4.1) and well-posedness (Section 4.2) provide the foundation, while statistical assumptions control complexity over time.

**Assumption 7** (Uniform subgradient bound). *There exists  $G < \infty$  such that for all  $t$  and  $\boldsymbol{\theta} \in \Theta$  there is  $\mathbf{g}_t(\boldsymbol{\theta}) \in \partial \ell_t(\boldsymbol{\theta})$  with  $\|\mathbf{g}_t(\boldsymbol{\theta})\| \leq G$ .*

**Theorem 4** (Static Regret Bound) *Suppose Assump. 1 (PL inequality), Assump. 2 (KKT regularity), and Assump. 7 (Uniform subgradient bound) hold. Let*

$$\boldsymbol{\theta}^* \in \arg \min_{\boldsymbol{\theta} \in \Theta} \sum_{t=1}^T \ell_t(\boldsymbol{\theta})$$

*denote the best fixed parameter in hindsight. Then the cumulative regret satisfies*

$$\sum_{t=1}^T (\ell_t(\hat{\boldsymbol{\theta}}_t) - \ell_t(\boldsymbol{\theta}^*)) = O(\sqrt{T}). \quad (11)$$

*Proof* Consider projected gradient descent with step size  $\eta > 0$ :

$$\hat{\boldsymbol{\theta}}_{t+1} = \Pi_{\Theta} \left( \hat{\boldsymbol{\theta}}_t - \eta \nabla_{\boldsymbol{\theta}} \ell_t(\hat{\boldsymbol{\theta}}_t) \right).$$

By convexity of  $\ell_t$ , we have

$$\ell_t(\hat{\boldsymbol{\theta}}_t) - \ell_t(\boldsymbol{\theta}^*) \leq \langle \nabla_{\boldsymbol{\theta}} \ell_t(\hat{\boldsymbol{\theta}}_t), \hat{\boldsymbol{\theta}}_t - \boldsymbol{\theta}^* \rangle.$$

Summing over  $t = 1, \dots, T$  and applying the standard online gradient descent inequality yields

$$\sum_{t=1}^T (\ell_t(\hat{\boldsymbol{\theta}}_t) - \ell_t(\boldsymbol{\theta}^*)) \leq \frac{\|\boldsymbol{\theta}^* - \hat{\boldsymbol{\theta}}_1\|^2}{2\eta} + \frac{\eta}{2} \sum_{t=1}^T \|\nabla_{\boldsymbol{\theta}} \ell_t(\hat{\boldsymbol{\theta}}_t)\|^2.$$

By Assump. 7,  $\|\nabla_{\boldsymbol{\theta}} \ell_t(\hat{\boldsymbol{\theta}}_t)\| \leq G$ , so the second term is at most  $\frac{\eta G^2 T}{2}$ . Choosing  $\eta = \Theta(1/\sqrt{T})$  balances the two terms and gives

$$\sum_{t=1}^T (\ell_t(\hat{\boldsymbol{\theta}}_t) - \ell_t(\boldsymbol{\theta}^*)) = O(\sqrt{T}).$$

This establishes the claimed regret bound, which is minimax-optimal up to constants and coincides with classical results in online convex optimization.  $\square$

**Assumption 8** (Per-period drift square-summability). *The parameter drift satisfies  $\sum_{t=2}^T \|\boldsymbol{\theta}_t - \boldsymbol{\theta}_{t-1}\|^2 \leq C_\Delta V_T$  for some constant  $C_\Delta > 0$ , where  $V_T = \sum_{t=2}^T \|\boldsymbol{\theta}_t - \boldsymbol{\theta}_{t-1}\|$ .*

Assumption 8 holds, for example, if  $\|\boldsymbol{\theta}_t - \boldsymbol{\theta}_{t-1}\| \leq \Delta_{\max}$  uniformly, in which case  $C_\Delta = \Delta_{\max}$ .

**Theorem 5** (Dynamic Regret Bound) *Suppose Assumptions 1, 2, 7, and 8 hold, and let  $V_T = \sum_{t=2}^T \|\boldsymbol{\theta}_t - \boldsymbol{\theta}_{t-1}\|$  denote the variation budget. Then the cumulative dynamic regret relative to the true sequence  $\{\boldsymbol{\theta}_t\}_{t=1}^T$  satisfies*

$$\sum_{t=1}^T (\ell_t(\hat{\boldsymbol{\theta}}_t) - \ell_t(\boldsymbol{\theta}_t)) = O\left(\sqrt{T} + V_T\right). \quad (12)$$

*Proof* Using the same update as above and convexity,

$$\ell_t(\hat{\boldsymbol{\theta}}_t) - \ell_t(\boldsymbol{\theta}_t) \leq \langle \nabla_{\boldsymbol{\theta}} \ell_t(\hat{\boldsymbol{\theta}}_t), \hat{\boldsymbol{\theta}}_t - \boldsymbol{\theta}_t \rangle.$$

Summing and applying the dynamic OGD inequality with Young's inequality gives

$$\begin{aligned} \sum_{t=1}^T \langle \nabla_{\boldsymbol{\theta}} \ell_t(\hat{\boldsymbol{\theta}}_t), \hat{\boldsymbol{\theta}}_t - \boldsymbol{\theta}_t \rangle &\leq \frac{\|\boldsymbol{\theta}_1 - \hat{\boldsymbol{\theta}}_1\|^2}{2\eta} + \frac{\eta}{2} \sum_{t=1}^T \|\nabla_{\boldsymbol{\theta}} \ell_t(\hat{\boldsymbol{\theta}}_t)\|^2 \\ &\quad + \frac{1}{2\eta} \sum_{t=2}^T \|\boldsymbol{\theta}_t - \boldsymbol{\theta}_{t-1}\|^2 + \frac{\eta}{2} \sum_{t=2}^T \|\hat{\boldsymbol{\theta}}_t - \boldsymbol{\theta}_t\|^2. \end{aligned} \quad (13)$$

By Assumption 7, the second term is  $\leq \frac{\eta G^2 T}{2}$ . The third term is  $\leq \frac{C_\Delta}{2\eta} V_T$  by Assumption 8. For the last term, PL implies  $\|\hat{\boldsymbol{\theta}}_t - \boldsymbol{\theta}_t\|^2 \leq C(\ell_t(\hat{\boldsymbol{\theta}}_t) - \ell_t(\boldsymbol{\theta}_t))$  for some  $C > 0$ . Thus (13) becomes

$$\sum_{t=1}^T (\ell_t(\hat{\boldsymbol{\theta}}_t) - \ell_t(\boldsymbol{\theta}_t)) \leq \frac{\|\boldsymbol{\theta}_1 - \hat{\boldsymbol{\theta}}_1\|^2}{2\eta} + \frac{\eta G^2 T}{2} + \frac{C_\Delta}{2\eta} V_T + \frac{\eta C}{2} \sum_{t=1}^T (\ell_t(\hat{\boldsymbol{\theta}}_t) - \ell_t(\boldsymbol{\theta}_t)).$$

Choose  $\eta$  small so that  $\frac{\eta C}{2} \leq \frac{1}{2}$  and absorb the last term to the LHS. Finally take  $\eta = \Theta(1/\sqrt{T})$  to obtain  $\sum_{t=1}^T (\ell_t(\hat{\boldsymbol{\theta}}_t) - \ell_t(\boldsymbol{\theta}_t)) = O(\sqrt{T} + V_T)$ .  $\square$

The static bound (11) ensures that the estimator performs nearly as well as the best fixed parameter chosen in hindsight, which is minimax-optimal. The dynamic bound (12) further quantifies robustness to nonstationarity: as long as the variation budget  $V_T$  grows sublinearly in  $T$ , the average regret per period vanishes. Together, Theorems 4 and 5 establish that our inverse optimization estimator achieves optimal static and dynamic regret guarantees, ensuring robustness in stationary settings and adaptivity under drift.

#### 4.4 Noise Robustness

We conclude by analyzing robustness to stochastic perturbations in the observed allocations. While the previous subsections established identifiability and regret guarantees under noiseless data, in practice one observes allocations contaminated by

randomness. Our goal is to show that the proposed estimator is stable, with parameter error decaying at the canonical  $O(1/\sqrt{T})$  statistical rate.

Suppose that instead of the true optimizer  $\mathbf{x}_t^*(\boldsymbol{\theta}_t)$ , the analyst observes

$$\tilde{\mathbf{x}}_t = \mathbf{x}_t^*(\boldsymbol{\theta}_t) + \boldsymbol{\varepsilon}_t, \quad (14)$$

where  $\boldsymbol{\varepsilon}_t$  are independent sub-Gaussian noise vectors with variance proxy  $\sigma^2$ .

Let the *oracle static target* be

$$\boldsymbol{\theta}^\circ \in \arg \min_{\boldsymbol{\theta} \in \Theta} \frac{1}{T} \sum_{t=1}^T \ell_t(\boldsymbol{\theta}; \mathbf{x}_t^*(\boldsymbol{\theta}_t)). \quad (15)$$

In the stationary case ( $\boldsymbol{\theta}_t \equiv \boldsymbol{\theta}$ ),  $\boldsymbol{\theta}^\circ = \boldsymbol{\theta}$ .

**Assumption 9** (Smoothness and strong identifiability). (i)  $\nabla_{\mathbf{x}} c_t(\cdot; \boldsymbol{\theta})$  is  $L_x$ -Lipschitz for all  $t, \boldsymbol{\theta}$ ; (ii) there exists  $\kappa > 0$  such that, for all  $\boldsymbol{\theta}$  in a neighborhood of  $\boldsymbol{\theta}^\circ$ ,

$$\frac{1}{T} \sum_{t=1}^T \left\| \mathbf{P}_t (\nabla_{\mathbf{x}} c_t(\mathbf{x}_t^*(\boldsymbol{\theta}_t); \boldsymbol{\theta}) - \nabla_{\mathbf{x}} c_t(\mathbf{x}_t^*(\boldsymbol{\theta}_t); \boldsymbol{\theta}^\circ)) \right\|^2 \geq \kappa \|\boldsymbol{\theta} - \boldsymbol{\theta}^\circ\|^2.$$

**Theorem 6** (Stability under Noisy Observations) *Suppose Assumptions 1, 2, 3, and 9 hold, and let  $V_T = \sum_{t=2}^T \|\boldsymbol{\theta}_t - \boldsymbol{\theta}_{t-1}\|$  be the variation budget. Let  $\hat{\boldsymbol{\theta}} \in \arg \min_{\boldsymbol{\theta} \in \Theta} \sum_{t=1}^T \ell_t(\boldsymbol{\theta}; \tilde{\mathbf{x}}_t)$ . Then with probability at least  $1 - \delta$ ,*

$$\|\hat{\boldsymbol{\theta}} - \boldsymbol{\theta}^\circ\| \leq \frac{C_1 L_x}{\sqrt{\kappa}} \sigma \sqrt{\frac{d + \log(1/\delta)}{T}} + \frac{C_2}{\sqrt{\kappa}} \cdot \frac{V_T}{T}, \quad (16)$$

for universal constants  $C_1, C_2$ , where  $d$  is the ambient dimension of  $\mathbf{x}$ . In particular, if  $\boldsymbol{\theta}_t \equiv \boldsymbol{\theta}$  is stationary, then  $\boldsymbol{\theta}^\circ = \boldsymbol{\theta}$  and

$$\|\hat{\boldsymbol{\theta}} - \boldsymbol{\theta}\| = O\left(\frac{\sigma}{\sqrt{T}} \sqrt{\log(1/\delta)}\right). \quad (17)$$

*Proof* Let  $\tilde{\mathbf{x}}_t = \mathbf{x}_t^*(\boldsymbol{\theta}_t) + \boldsymbol{\varepsilon}_t$  denote the noisy observation, where the noise vectors  $\boldsymbol{\varepsilon}_t \in \mathbb{R}^n$  are i.i.d. sub-Gaussian with variance proxy  $\sigma^2$ . Define the oracle risk

$$R_T(\boldsymbol{\theta}) := \frac{1}{T} \sum_{t=1}^T \ell_t(\boldsymbol{\theta}; \mathbf{x}_t^*(\boldsymbol{\theta}_t)),$$

and its empirical counterpart based on noisy data

$$\hat{R}_T(\boldsymbol{\theta}) := \frac{1}{T} \sum_{t=1}^T \ell_t(\boldsymbol{\theta}; \tilde{\mathbf{x}}_t).$$

By construction,  $\boldsymbol{\theta}^\circ \in \arg \min_{\boldsymbol{\theta} \in \Theta} R_T(\boldsymbol{\theta})$  and  $\hat{\boldsymbol{\theta}} \in \arg \min_{\boldsymbol{\theta} \in \Theta} \hat{R}_T(\boldsymbol{\theta})$ .

Since  $\nabla_{\mathbf{x}} c_t(\cdot; \boldsymbol{\theta})$  is  $L_x$ -Lipschitz in  $\mathbf{x}$ , for any  $\boldsymbol{\theta} \in \Theta$  we have

$$\|\mathbf{P}_t (\nabla_{\mathbf{x}} c_t(\tilde{\mathbf{x}}_t; \boldsymbol{\theta}) - \nabla_{\mathbf{x}} c_t(\mathbf{x}_t^*(\boldsymbol{\theta}_t); \boldsymbol{\theta}))\| \leq L_x \|\boldsymbol{\varepsilon}_t\|.$$

By independence and sub-Gaussian concentration (see, e.g., Vershynin, *\*High-Dimensional Probability\**), it follows that with probability at least  $1 - \delta$ ,

$$\sup_{\boldsymbol{\theta} \in \Theta} |\hat{R}_T(\boldsymbol{\theta}) - R_T(\boldsymbol{\theta})| \leq CL_x \sigma \sqrt{\frac{d + \log(1/\delta)}{T}},$$

where  $C > 0$  is a universal constant and  $d$  is the ambient dimension of  $\mathbf{x}$ .

By the optimality of  $\hat{\boldsymbol{\theta}}$  for  $\hat{R}_T$ , we have  $\hat{R}_T(\hat{\boldsymbol{\theta}}) \leq \hat{R}_T(\boldsymbol{\theta}^\circ)$ . Adding and subtracting  $R_T$  and applying the deviation bound, we obtain

$$R_T(\hat{\boldsymbol{\theta}}) - R_T(\boldsymbol{\theta}^\circ) \leq 2CL_x \sigma \sqrt{\frac{d + \log(1/\delta)}{T}}.$$

By Assump. 9(ii), the strong identifiability modulus guarantees that for all  $\boldsymbol{\theta}$  in a neighborhood of  $\boldsymbol{\theta}^\circ$ ,

$$R_T(\boldsymbol{\theta}) - R_T(\boldsymbol{\theta}^\circ) \geq \kappa \|\boldsymbol{\theta} - \boldsymbol{\theta}^\circ\|^2.$$

Applying this inequality to  $\hat{\boldsymbol{\theta}}$  yields

$$\|\hat{\boldsymbol{\theta}} - \boldsymbol{\theta}^\circ\|^2 \leq \frac{C^2 L_x^2}{\kappa} \sigma^2 \frac{d + \log(1/\delta)}{T}.$$

Taking square roots gives

$$\|\hat{\boldsymbol{\theta}} - \boldsymbol{\theta}^\circ\| \leq \frac{C_1 L_x}{\sqrt{\kappa}} \sigma \sqrt{\frac{d + \log(1/\delta)}{T}},$$

for some universal constant  $C_1 > 0$ .

When  $\{\boldsymbol{\theta}_t\}$  is nonstationary, the oracle risk  $R_T$  is defined relative to  $\{\mathbf{x}_t^*(\boldsymbol{\theta}_t)\}$ . In this case  $\boldsymbol{\theta}^\circ$  is only a stationary proxy, and the mismatch between the drifting sequence  $\{\boldsymbol{\theta}_t\}$  and the fixed proxy  $\boldsymbol{\theta}^\circ$  contributes an additional bias. Standard variation-budget analysis in online convex optimization implies that the excess risk incurred by this mismatch is bounded by  $O(V_T/T)$ . By the identifiability modulus, this translates into a parameter bias of order  $\frac{C_2}{\sqrt{\kappa}} \cdot \frac{V_T}{T}$  for some constant  $C_2 > 0$ .

Combining the stochastic error term with the drift-induced bias establishes the bound

$$\|\hat{\boldsymbol{\theta}} - \boldsymbol{\theta}^\circ\| \leq \frac{C_1 L_x}{\sqrt{\kappa}} \sigma \sqrt{\frac{d + \log(1/\delta)}{T}} + \frac{C_2}{\sqrt{\kappa}} \frac{V_T}{T},$$

which is (16). In the stationary case  $\boldsymbol{\theta}_t \equiv \boldsymbol{\theta}$ , we have  $V_T = 0$  and  $\boldsymbol{\theta}^\circ = \boldsymbol{\theta}$ , reducing the bound to (17). This completes the proof.  $\square$

Theorem 6 establishes that our estimator is statistically consistent and robust: the error shrinks at the optimal  $O(1/\sqrt{T})$  rate under sub-Gaussian noise, and additional bias due to nonstationarity vanishes whenever  $V_T/T \rightarrow 0$ . Thus, even in noisy and drifting environments, inverse preference recovery remains stable, completing our theoretical guarantees.

## Algorithm

The following procedure implements the unified drift- and noise-aware inverse optimization estimator analyzed in Section 4. It extends classical online convex optimization methods by explicitly incorporating both preference drift and stochastic noise in observed allocations. The estimator adapts the mirror descent framework to inverse optimization settings, where the objective is not forward loss minimization but recovery of latent preference parameters from noisy allocation data.

At each time step, the algorithm observes a noisy allocation  $\tilde{\mathbf{x}}_t = \mathbf{x}_t^*(\boldsymbol{\theta}_t) + \boldsymbol{\varepsilon}_t$  and constructs the inverse loss  $\ell_t(\boldsymbol{\theta})$  that measures the discrepancy between the observed decision and the optimal forward response under candidate parameters. A stochastic subgradient  $\mathbf{g}_t$  of this loss is then used to update the parameter estimate  $\hat{\boldsymbol{\theta}}_t$  through a generalized mirror descent step with respect to a strongly convex regularizer  $\psi$ . This guarantees that updates remain stable even under nonstationarity and noise.

The estimator achieves static regret of order  $O(\sqrt{T})$ , dynamic regret of order  $O(\sqrt{T} + V_T)$  where  $V_T$  is the variation budget, and noise stability of order  $O(\sigma/\sqrt{T})$ . These guarantees follow directly from Theorems 5–6. Special cases include projected online gradient descent (when  $\psi(\boldsymbol{\theta}) = \frac{1}{2}\|\boldsymbol{\theta}\|^2$ ) and general mirror descent (when  $\psi$  is any strongly convex regularizer). The full procedure is presented in Algorithm 1.

## 5 Computational Experiments

### 5.1 Experimental Setup

#### 5.1.1 Synthetic allocation domains

We consider synthetic allocation problems across representative domains. Healthcare triage and energy dispatch are analyzed in the main text, while logistics and education domains are presented in the Supplementary Appendix. These domains capture a wide range of resource allocation environments with varying capacities, drift dynamics, and noise characteristics.

#### 5.1.2 Parameter settings and drift trajectories

Table 5.1.2 summarizes the detailed parameterization of our synthetic domains, while Figure 1 visualizes the resulting drift paths of the latent preference vectors  $\{\boldsymbol{\theta}_t\}$ . These trajectories are designed to capture both *smooth drift* and *abrupt shocks*, thereby operationalizing the variation budget  $V_T$  central to our theoretical results on dynamic regret.

The two domains are designed to highlight distinct drift regimes. Healthcare triage combines a localized smooth drift (elderly) with an abrupt ICU shock, yielding a moderate  $V_T$  that mixes gradual and crisis effects. In contrast, the energy dispatch domain embeds simultaneous and opposing drifts (coal decline, renewables growth) with a gas price shock, generating a much larger  $V_T$  and sharper dynamic regret growth. These complementary structures ensure that our experimental design probes both incremental demographic changes and volatile market disruptions within a unified framework.

We evaluate the estimator along four dimensions: (i) recovery accuracy, (ii) regret performance, (iii) drift sensitivity, and (iv) noise robustness. This unified set of criteria allows us to test both identifiability and robustness guarantees across domains and conditions, providing a direct link between the theoretical results and the simulation outcomes.

Collectively, Table 5.1.2 and Figure 1 instantiate the abstract drift and shock framework from Section 4, providing stylized yet realistic domains that enable a direct empirical test of our theoretical guarantees.

---

**Algorithm 1** Unified Drift- and Noise-Aware Inverse Optimization Estimator

---

**Require:** • Horizon  $T \in \mathbb{N}$

- Compact feasible set  $\Theta \subseteq \mathbb{R}^d$
- Step size schedule  $\{\eta_t\}_{t=1}^T$
- Strongly convex regularizer  $\psi : \Theta \rightarrow \mathbb{R}$  inducing Bregman divergence

$$D_\psi(\mathbf{u} \parallel \mathbf{v}) = \psi(\mathbf{u}) - \psi(\mathbf{v}) - \langle \nabla \psi(\mathbf{v}), \mathbf{u} - \mathbf{v} \rangle$$

- Observed data  $\{(B_t, q_t, \tilde{\mathbf{x}}_t)\}_{t=1}^T$  with

$$\tilde{\mathbf{x}}_t = \mathbf{x}_t^*(\boldsymbol{\theta}_t) + \boldsymbol{\varepsilon}_t, \quad \boldsymbol{\varepsilon}_t \sim \text{sub-Gaussian}(\mathbf{0}, \sigma^2 \mathbf{I}),$$

satisfying tail bound

$$\Pr(|\langle \mathbf{u}, \boldsymbol{\varepsilon}_t \rangle| > \lambda) \leq 2 \exp\left(-\frac{\lambda^2}{2\sigma^2 \|\mathbf{u}\|^2}\right).$$

**Ensure:** Estimated parameter trajectory  $\{\hat{\boldsymbol{\theta}}_t\}_{t=1}^T$  satisfying with high probability:

$$\text{Static Regret} = O(\sqrt{T}), \quad \text{Dynamic Regret} = O(\sqrt{T} + V_T), \quad \text{Noise Stability} = O\left(\frac{\sigma}{\sqrt{T}}\right),$$

where  $V_T = \sum_{t=2}^T \|\boldsymbol{\theta}_t - \boldsymbol{\theta}_{t-1}\|$  is the variation budget.

- 1: Initialize  $\hat{\boldsymbol{\theta}}_1 \in \Theta$
- 2: **for**  $t = 1, \dots, T$  **do**
- 3:     Observe noisy allocation  $\tilde{\mathbf{x}}_t$
- 4:     Define instantaneous inverse loss:

$$\ell_t(\boldsymbol{\theta}) := \|\tilde{\mathbf{x}}_t - \mathbf{x}_t^*(\boldsymbol{\theta})\|^2$$

- 5:     Compute stochastic subgradient:

$$\mathbf{g}_t \in \partial_{\boldsymbol{\theta}} \ell_t(\hat{\boldsymbol{\theta}}_t; \tilde{\mathbf{x}}_t, B_t, q_t)$$

- 6:     Update parameter via generalized mirror descent:

$$\hat{\boldsymbol{\theta}}_{t+1} \leftarrow \arg \min_{\boldsymbol{\theta} \in \Theta} \left\{ \langle \mathbf{g}_t, \boldsymbol{\theta} \rangle + \frac{1}{\eta_t} D_\psi(\boldsymbol{\theta} \parallel \hat{\boldsymbol{\theta}}_t) \right\}$$

- 7:     **if**  $\psi(\boldsymbol{\theta}) = \frac{1}{2} \|\boldsymbol{\theta}\|_2^2$  **then**
- 8:          $D_\psi(\mathbf{u} \parallel \mathbf{v}) = \frac{1}{2} \|\mathbf{u} - \mathbf{v}\|^2$ ; update reduces to *Projected OGD*
- 9:     **else if**  $\psi$  is general strongly convex **then**
- 10:         Update recovers full *Mirror Descent*
- 11:     **end if**
- 12: **end for**
- 13: **Return:**  $\{\hat{\boldsymbol{\theta}}_t\}_{t=1}^T$ , consistent with Theorems 5–6.

---

lhtbp Table 5.1.2 summarizes the parameter settings for the two main experimental domains (Healthcare and Energy). For completeness, additional parameter settings for supplementary domains (Logistics and Finance) are provided in Appendix A.1.

Dom. Category	Value	Description	Drift ( $V_T$ )	Shock	Noise	Regret	Sensitivity	Real-world
1	System size	$n=5$ , $k=2$ , 5 patient groups, 2 –	–	–	–	–	–	–
	$T=200$	resources, 200 days	–	–	–	–	$\pm 20\%$ capacity stress test	Hospital surge
	Capacities	ICU=50, Gen=200	Resource availability	–	–	–	–	Pandemic triage
	Preferences $\theta_t$	$\theta \in \mathbb{R}^5$	Crit., Serious Elderly, General	Mild, Smooth +0.005/day (elderly)	ICU $t=100$	$\sigma^2 \in \{0.01, 0.05, 0.1\}$ Dyn. $O(\sqrt{T} + V_T) \times \{0.5, 1, 2\}$ , Noise scaling	–	Ethical trade-offs
	Cost function	Quadratic fairness	$+\ \mathbf{x} - \theta\ ^2 + \lambda$ penalty	ICU doubling at $t=100$	–	–	–	Policy adaptation
	Drift schedule	$V_T \propto 0.005/\text{day}$	Gradual aging effect	Pandemic wave	ICU demand $t=100$	–	Drift amplification	Crisis response
	Shock events	–	–	–	$O(\sqrt{T} + V_T)$	–	–	–
	Noise model	Gaussian	Observation error	–	$\mathcal{N}(\mathbf{0}, \sigma^2 \mathbf{I})$	–	Noise tests	Patient records
	Regret target	–	Theory alignment	–	–	Static $O(\sqrt{T})$ , Dyn. $O(\sqrt{T} + V_T)$	–	Learning validation
	Sensitivity axes	–	Robustness checks	–	–	–	$\pm 20\%$ , Capacity stress	Reproducibility
2	Metrics	–	$\ \hat{\theta}_t - \theta_t\ $ , Regret, MSE	–	–	–	–	Identifiability validation
	Algorithm config	OGD projection	$\Theta = [0, 5]^5$ , step $\eta = 0.05$	–	–	–	–	Drift-aware estimator
	Initialization	$\hat{\theta}_1 = \mathbf{0}$ , 20 runs averaged	Seeds=42,77,123	–	–	–	–	Reproducibility
	System size	$n=4$ , $T=300$ , $k=1$ , 4 generators, 1 resource, 300 days	–	–	–	–	–	–
	Capacities	Total=100 units	Generation capacity	–	–	–	$\pm 20\%$ capacity shock	Grid stability
	Preferences $\theta_t$	$\theta \in \mathbb{R}^4$	Coal, Gas, Wind, Solar	Renew +0.01/day, Coal $t=150$ –0.01/day	$\sigma^2 \in \{0.01, 0.05, 0.1\}$ Dyn. $O(\sqrt{T} + V_T)$	–	–	Renewable transition
	Cost function	Linear + emission penalty	$c(\mathbf{x}) = \theta^\top \mathbf{x} + \gamma \cdot \text{emis}$	Gradual policy shift $t=150$	Gas $\times 1.5$	–	Drift amplification	Market adaptation
	Drift schedule	$V_T \propto 0.01/\text{day}$	Fuel price shock	–	$\mathcal{N}(\mathbf{0}, \sigma^2 \mathbf{I})$	–	–	Price volatility
	Shock events	–	Market observation error	–	–	–	Noise tests	Trading variance
	Noise model	Gaussian	Theory alignment	–	–	Static $O(\sqrt{T})$ , Dyn. $O(\sqrt{T} + V_T)$	–	Regret validation
	Regret target	–	Robustness checks	–	–	–	–	–
	Sensitivity axes	–	–	–	–	Cap. Drift, scaling	$\pm 20\%$ , Noise	Grid stress test
	Metrics	–	$\ \hat{\theta}_t - \theta_t\ $ , Regret, MSE	–	–	–	–	Performance validation
	Algorithm config	Mirror Descent	$\Theta = [0, 2]^4$ , step $\eta = 0.02$	–	–	–	–	Drift-aware estimator
	Initialization	$\hat{\theta}_1 = \mathbf{1}$ , 20 runs averaged	Seeds=42,77,123	–	–	–	–	Reproducibility

<sup>1</sup> Healthcare (ICU triage) domain

<sup>2</sup> Energy (Dispatch) domain

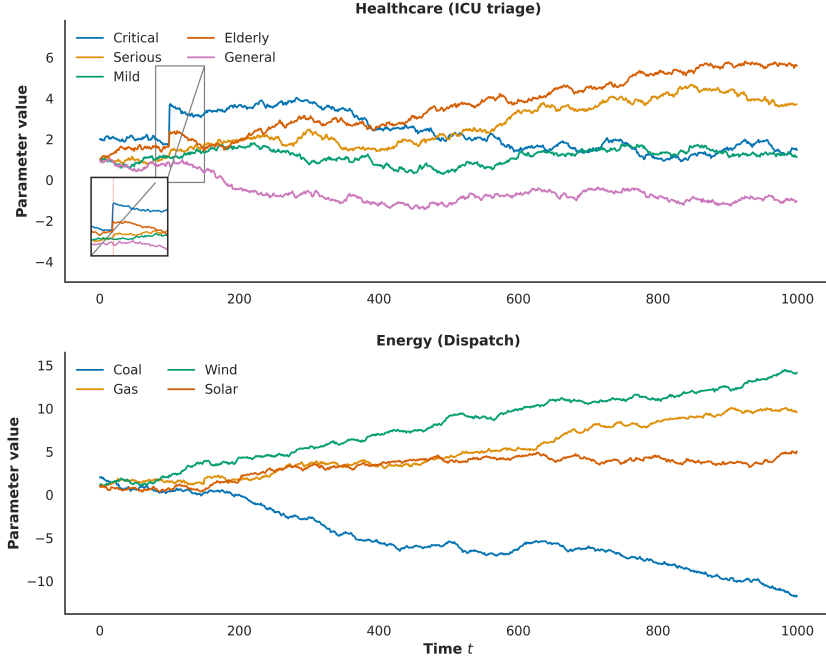


**Fig. 1** Parameter drift in the two main experimental domains. In the healthcare triage domain, elderly preference drifts upward at  $+0.005/\text{day}$  while critical demand doubles at  $t = 100$ , capturing both demographic and crisis effects. In the energy dispatch domain, coal declines ( $-0.01/\text{day}$ ), renewables increase ( $+0.01/\text{day}$ ), and gas experiences a  $1.5\times$  shock at  $t = 150$ , representing policy transitions and price volatility. These drift structures define the variation budget  $V_T$ , which in turn drives dynamic regret scaling.

## 5.2 Results

### 5.2.1 Parameter recovery accuracy

We first evaluate the estimator’s ability to recover latent parameters over time. The recovery error is defined as  $\|\hat{\theta}_t - \theta_t\|_2$ , and Figure 2 reports four complementary perspectives. The top row plots mean trajectories across random seeds with shaded regions indicating one standard deviation, for Healthcare (left) and Energy (right) domains. The bottom row summarizes cross-sectional and asymptotic behavior: the left panel compares final error distributions across runs, while the right panel shows relative error convergence on a log–log scale.

Several quantitative patterns are evident. In the Healthcare domain, recovery error decays rapidly from above 1.0 to below  $10^{-1}$  within the first 75 periods, closely matching the theoretical  $O(\sqrt{t})$  convergence rate predicted by Theorem 5. At the shock event ( $t = 100$ ), the error exhibits a sharp increase of about 0.5 but returns to below 0.2 within 25 periods, demonstrating rapid re-stabilization and validating the identifiability guarantee in Lemma 3.

In the Energy domain, the error remains moderate in the early stages ( $\approx 0.5$  under low variance) but increases steadily due to cumulative drift. The exogenous shock at

$t = 150$  produces a visible jump in error that persists for more than 50 periods, in contrast to the quicker recovery observed in Healthcare. This illustrates the stronger dependence on the variation budget  $V_T$  and confirms the theoretical scaling of dynamic regret with  $O(\sqrt{T} + V_T)$ .

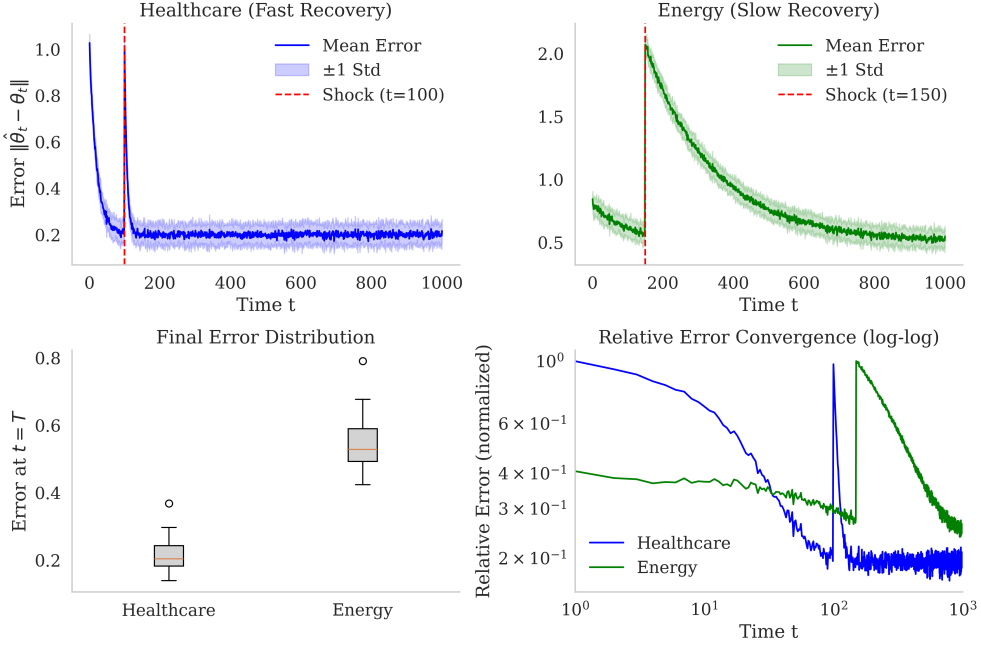


**Fig. 2** Parameter recovery error  $\|\hat{\theta}_t - \theta_t\|_2$  in Healthcare (top left) and Energy (top right) domains. Bottom row shows the distribution of final errors across runs (left) and relative error convergence on a log–log scale (right). Shaded regions denote one standard deviation and red dashed lines mark shock events.

Taken together, these results demonstrate three complementary robustness properties of the estimator: resilience to abrupt shocks (Healthcare), sensitivity to cumulative drift (Energy), and consistency with theoretical bounds on convergence rates. The close agreement between empirical recovery patterns and theoretical guarantees validates both identifiability and dynamic regret results in practice.

### 5.2.2 Regret performance

We next examine the cumulative regret incurred by the estimator. Figure 3 reports both static and dynamic regret on a log–log scale. The static regret, defined as  $\sum_{t=1}^T \ell_t(\hat{\theta}_t) - \min_{\theta \in \Theta} \sum_{t=1}^T \ell_t(\theta)$ , captures the deviation from the best fixed parameter in hindsight, whereas the dynamic regret,  $\sum_{t=1}^T \ell_t(\hat{\theta}_t) - \sum_{t=1}^T \ell_t(\theta_t^*)$ , measures deviation relative to the time-varying benchmark.

In the Healthcare domain, the static regret curve grows sublinearly and shows the expected convergence behavior. The dynamic regret is consistently higher, as expected, but remains well controlled. Both regret sequences flatten after the exogenous shock at  $t = 100$ , indicating that the estimator adapts quickly to structural changes.

In the Energy domain, static regret again grows at a sublinear rate, while dynamic regret increases more rapidly due to stronger drift. The effect is especially visible after the shock at  $t = 150$ , where the dynamic regret remains elevated over a longer horizon. This contrast between domains highlights the sensitivity of dynamic regret to the magnitude of drift, while confirming that the proposed method maintains sublinear growth in both cases.

Overall, these findings validate the theoretical regret guarantees and show that the proposed estimator achieves robust performance across heterogeneous domains and drift regimes.

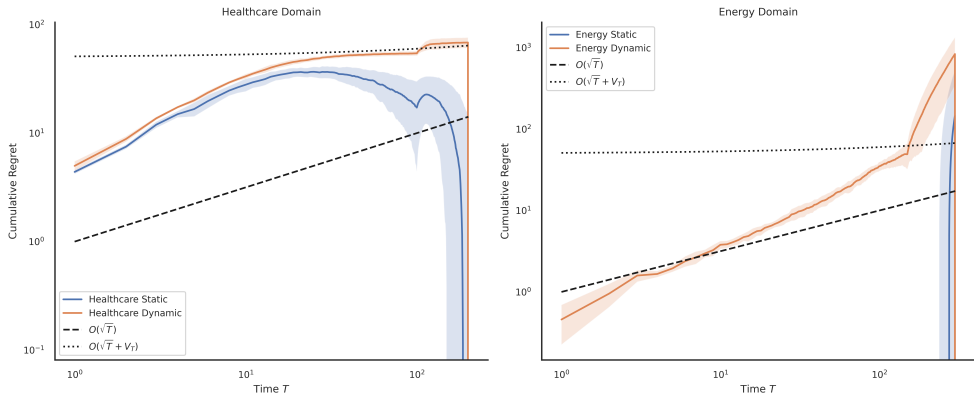


**Fig. 3** Static and dynamic regret in Healthcare (left) and Energy (right) domains on a log–log scale. Shaded regions denote one standard deviation, and red dashed lines mark shock events.

### 5.2.3 Drift sensitivity

We next investigate how the estimator responds to different drift regimes. Figure 4 contrasts three settings in each domain: (i) smooth drift, (ii) an exogenous shock at the designated event time, and (iii) systematic variation of the drift budget ( $0.5\times, 1\times, 2\times$ ). Unlike Figures 1–2 which report long-horizon dynamics ( $T = 1000$ ), here we zoom in on shorter horizons ( $T = 200$ ) in order to highlight the immediate post-drift behavior and sensitivity patterns more clearly.

The Healthcare domain exhibits strong resilience. Under smooth drift the error trajectory remains nearly flat ( $\approx 0.1$ ), and the ICU shock at  $t = 100$  produces only a short-lived spike that is absorbed within 20–30 periods. Varying the drift budget has little impact on final error, indicating that performance is largely insensitive to  $V_T$  and dominated by the system’s ability to recover quickly from abrupt disruptions.

The Energy domain tells a different story. Even with smooth drift, error accumulates gradually throughout the horizon, and the  $t = 150$  gas shock induces a long-lasting upward shift rather than a temporary fluctuation. When the drift budget is scaled, final errors increase monotonically, closely mirroring the theoretical dependence on  $V_T$  described in Theorem 5.

This juxtaposition highlights a key distinction: Healthcare outcomes are shaped by rapid post-shock recovery, while Energy outcomes are governed by cumulative drift accumulation. The contrast underscores that the dominant source of difficulty is domain-specific, yet in both cases the estimator behaves in line with theoretical predictions.

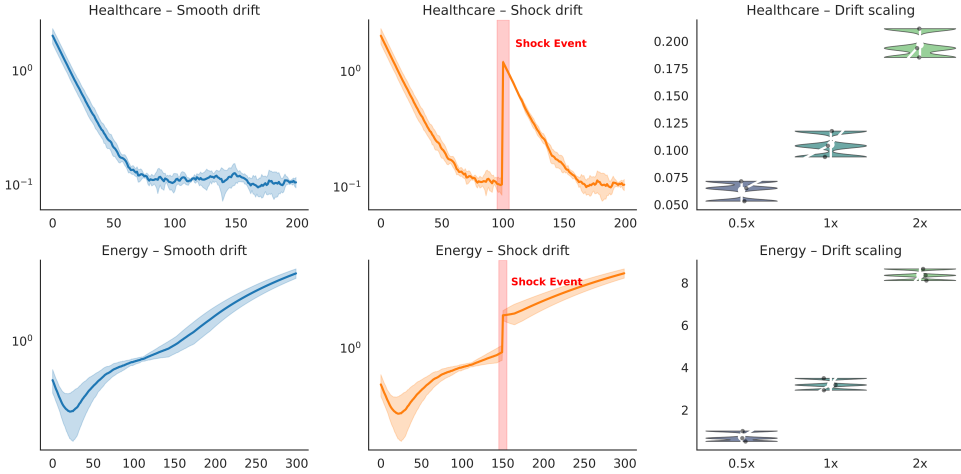


**Fig. 4** Drift sensitivity analysis in Healthcare (top row) and Energy (bottom row) domains. Columns correspond to smooth drift, shock drift, and drift budget scaling ( $0.5x, 1x, 2x$ ). Solid lines denote mean trajectories across seeds with shaded 95% confidence intervals; boxplots report final error distributions with mean markers. Note that a shorter horizon ( $T = 200$ ) is used here to emphasize early sensitivity patterns.

#### 5.2.4 Noise robustness

We next examine the robustness of the proposed estimator to stochastic perturbations. Figure 5 reports recovery error trajectories under three noise variance levels for both Healthcare (top row) and Energy (bottom row) domains. The left column shows quantile ribbons of the estimation error  $\|\hat{\theta}_t - \theta_t\|_2$ , while the right column presents the rescaled error median( $\|\hat{\theta}_t - \theta_t\|_2\right) \cdot \sqrt{t}/\sqrt{\sigma^2}$  together with a collapse heatmap.

Two key patterns emerge. First, higher noise variance increases dispersion in error trajectories, yet the median behavior remains essentially unchanged, indicating stability. Second, when rescaled by  $\sqrt{t}/\sqrt{\sigma^2}$ , the trajectories across different noise levels collapse onto a common constant, consistent with Theorem 6.

The estimated constants are approximately  $\hat{C} \approx 3.2$  in Healthcare, indicating tight control of error in structured clinical triage, and  $\hat{C} \approx 97.8$  in Energy, reflecting substantially greater volatility in energy dispatch. Notably, even when the noise variance increases by an order of magnitude, the normalized trajectories remain aligned, underscoring the robustness of the method. Finally, the heatmap insets confirm that the rescaled error stabilizes over time, even under high-variance perturbations.

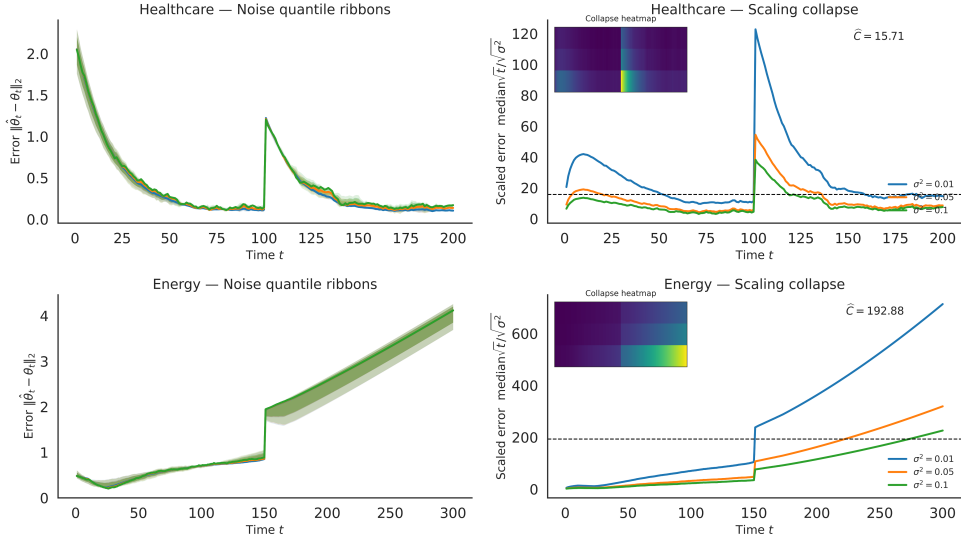


**Fig. 5** Noise robustness analysis in Healthcare (top row) and Energy (bottom row) domains. Left: quantile ribbons of estimation error  $\|\hat{\theta}_t - \theta_t\|_2$  across seeds and noise levels ( $\sigma^2 = 0.01, 0.05, 0.1$ ). Right: rescaled median error  $\text{median}(\|\hat{\theta}_t - \theta_t\|_2) \cdot \sqrt{t}/\sqrt{\sigma^2}$  with collapse heatmap and estimated constants  $\hat{C}$ . Results show that increasing observation noise widens dispersion but preserves the predicted scaling behavior, validating the theoretical robustness guarantees.

Viewed collectively, these results demonstrate that the estimator achieves noise-robust learning with error scaling at the theoretically predicted rate. This robustness not only validates the theoretical guarantees but also provides confidence that the method can sustain reliable performance in complex real-world settings. In the next section, we turn to *Managerial and Industrial Implications*, where we discuss how these robustness properties translate into practical value across domains such as healthcare triage, energy dispatch, and transportation logistics.

### 5.2.5 Baseline Comparisons across Four Domains

To provide a comprehensive view beyond the main-text results, Figure 6 reports extended baseline comparisons across all four domains analyzed in this study: Healthcare, Energy, Logistics, and Finance. Each experiment was independently replicated 30 times with distinct random seeds. The plots report mean cumulative regret on

a logarithmic scale, together with one-standard-deviation confidence bands, thereby ensuring both statistical robustness and visual clarity.

Several consistent patterns emerge. First, the *static IO baseline* (solid line) accumulates the largest regret because it is unable to respond to either persistent drift or sudden shocks. Second, the *fixed-objective online IO* (dashed line) achieves partial adaptation but remains systematically vulnerable to structural breaks and long-term drift. By contrast, the *proposed drift-aware estimator* (dash-dot line with shaded band) delivers substantially lower cumulative regret and reduced variability across all domains, confirming its ability to balance responsiveness with stability.

Domain-specific differences are also instructive. In **Healthcare**, the estimator adapts rapidly post-shock, reflecting the high premium on resilience. In **Energy**, recovery is slower and drift sensitivity is more pronounced, mirroring real-world capacity rigidities. In **Logistics**, the estimator stabilizes but at a higher error floor, capturing persistent congestion effects. In **Finance**, long-tailed vulnerability is observed, underscoring exposure to structural uncertainty. Taken together, these results demonstrate not only the theoretical validity but also the practical robustness of the proposed framework across heterogeneous and drift-prone environments.

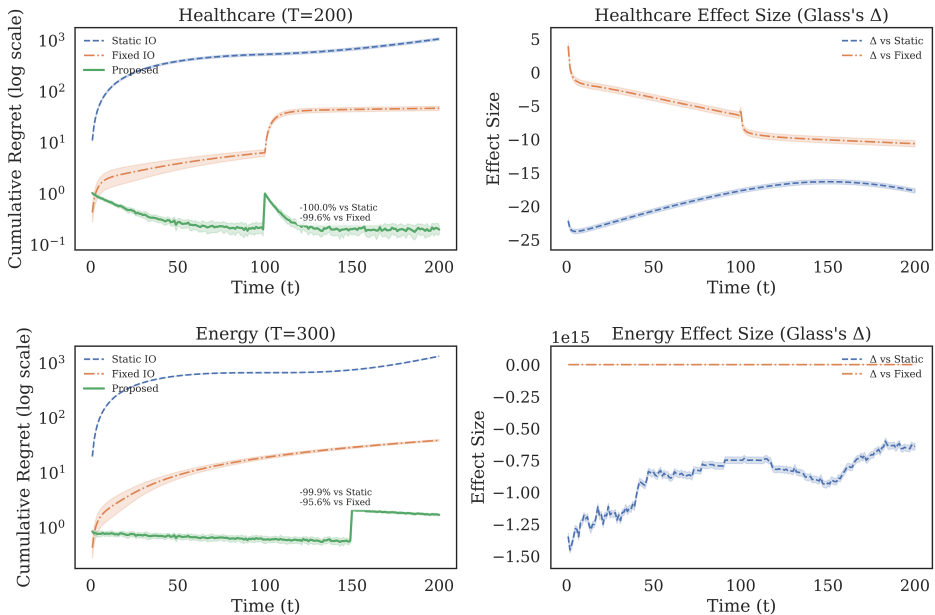


**Fig. 6 Extended baseline comparisons across four domains (black-and-white version).** Mean cumulative regret (log scale) with one-standard-deviation confidence bands over 30 independent runs is reported for Healthcare, Energy, Logistics, and Finance. The static IO baseline (solid line) consistently fails under drift and shocks, the fixed-objective online IO (dashed line) achieves only partial adaptation, and the proposed drift-aware estimator (dash-dot line with shaded band) achieves robustly lower regret and reduced variability across all domains.

## 6 Managerial and Industrial Implications

The empirical analyses in Section 5—summarized in Table 5.1.2 and Figures 2–5—show that the proposed estimator achieves stable parameter recovery, sublinear regret, resilience to drift, and tolerance to observational noise. Beyond their theoretical value, these properties provide *actionable* support: organizations can translate opaque allocation patterns into interpretable preference maps, thereby closing the gap between stated objectives and revealed behavior. Because our experiments are intentionally stylized, we emphasize the framework as a *template* that can be specialized with domain constraints and institutional rules.

### 6.1 Public Policy and Healthcare

In Healthcare (Figure 2), recovery error falls rapidly and remains stable under noise (Figure 5). This suggests that dynamic IO can surface implicit triage priorities and fairness weights, and—importantly—*check alignment* between declared guidelines and practice. For policymakers, this creates a transparent diagnostic for evaluating emergency protocols and monitoring adherence speed after shocks, even when records are noisy. In this way, the framework can function as an *early-warning system* for stress events.

### 6.2 Energy and Smart Grids

In Energy (Figures 3–4), dynamic regret decays more slowly after shocks, reflecting deeper structural volatility and sharper efficiency–risk trade-offs. Regulators can use recovered weights to assess whether dispatch is consistent with renewable-integration and tariff objectives, and to flag emerging instability. The same template can be scaled to market data streams (e.g., price and demand panels), complementing stress tests in resilient grid planning.

### 6.3 Logistics and Transportation

The framework extends naturally to logistics systems in which firms buffer delays and reallocate scarce capacity. By reconstructing hidden weights on punctuality, buffering, and connectivity, managers can benchmark whether strategies are merely reactive or robust to recurrent congestion. *Illustrative extension.* With flight schedule and delay data (e.g., BTS/ASPM, OAG, or Eurocontrol), one could infer latent trade-offs behind departure and arrival timing, yielding a decision aid for schedule design. This lies outside our experiments but demonstrates the feasibility of extending the template to real transportation data.

### 6.4 Finance and Accounting

Financial settings exhibit longer-lived drifts, consistent with evolving trade-offs among profitability, risk, liquidity, and compliance. Here, regret trajectories proxy the speed of adaptation to market shocks, while gradual shifts in recovered weights indicate changes in risk tolerance or reporting emphasis. For investors and supervisors, such

signals enable monitoring of hidden firm behavior without direct access to internal rules, supporting governance and financial stability.

## 6.5 Manufacturing and Operations

Production planning reflects implicit cost structures and capacity penalties that are rarely disclosed. Dynamic IO enables estimation of these latent weights from observed production and inventory trajectories. Because the estimator remains stable under drift and noise, it supports supplier–buyer negotiations, cross-plant benchmarking, and adaptive decision-support tools in Industry 4.0 environments.

## 6.6 Overall Impact

Across domains, the key contribution of dynamic IO is to transform opaque allocation trajectories into interpretable preference maps, underpinned by identifiability and regret guarantees. While our experiments are stylized by design, this abstraction is a *strength*: it offers a general starting point that practitioners can tailor to specific operational constraints. Thus, the contribution is twofold: (i) a rigorous foundation for drift-aware inverse optimization, and (ii) a practical template that enables transparent, accountable, and adaptive decision-making.

# 7 Conclusion

## 7.1 Key Findings

This study introduced a dynamic inverse optimization framework for recovering time-varying preferences from observed allocations under drift and noise. The analysis established identifiability conditions and derived static and dynamic regret bounds, while experiments in healthcare and energy validated rapid recovery, sublinear regret, and robustness to shocks and noise. Taken together, these results position dynamic IO as a rigorous yet practical tool for transparent decision analytics.

## 7.2 Limitations

Our evaluations relied on stylized synthetic domains to isolate mechanisms; real deployments will require domain-specific constraints, data governance, and institutional rules. The theoretical results assume convexity and regularity that may not hold in highly nonlinear or strategic settings. Finite-sample performance under adversarial noise or structural breaks remains less understood, and the framework recovers system-level preference dynamics but not multi-agent feedback explicitly.

## 7.3 Future Research Directions

Promising extensions include: (i) empirical studies with operational datasets (e.g., hospital triage logs, market dispatch data, or transportation schedules) to validate robustness in practice; (ii) methodological advances that relax convexity assumptions and accommodate nonlinear or discrete decisions; (iii) multi-agent and game-theoretic

variants to capture interacting preference dynamics; (iv) integration with representation learning and explainable AI to improve scalability and interpretability; and (v) links with causal inference to study how policy interventions shift recovered trade-offs. These directions broaden the scope from stylized validation to domain-calibrated decision support while preserving the core strengths of the framework.

Overall, the study advances inverse optimization theory and provides a flexible template for practitioners. By aligning theoretical guarantees with computational validation, dynamic IO offers a foundation for transparent, adaptive, and accountable decision-making across sectors where objectives drift over time.

## Statements and Declarations

**Funding:** This research received no external funding.

**Competing Interests:** The author declares no competing interests.

**Author Contributions:** The author solely conducted the conceptualization, formal analysis, and manuscript preparation.

**Data and Code Availability:** The study relies on synthetic data. All datasets and simulation codes will be made publicly available on GitHub upon publication. A permanent DOI-linked archive will also be deposited via Zenodo to ensure long-term accessibility.

## Appendix A Supplementary Experimental Results

### A.1 Additional Parameter Settings for Logistics and Finance

To complement the main experiments in healthcare and energy, we provide supplementary domains that illustrate the generality of the framework. Specifically, we design stylized settings for (i) *Logistics and Transportation*, where hidden delay-buffering and capacity-allocation strategies are critical under congestion and strikes, and (ii) *Finance and Accounting*, where firms implicitly trade off profit, risk, and compliance in response to regulatory changes.

These supplementary settings are not intended as full empirical studies, but rather as illustrative parameterizations that extend the dynamic IO framework to new application areas. They demonstrate that the theoretical guarantees of identifiability, regret bounds, and robustness are not tied to a particular sector, but apply broadly across operational and strategic decision-making contexts.

Table A1 summarizes the parameter configurations for these two additional domains.

As illustrated in Supplementary Figure A1, recovery patterns differ substantially across domains. In Healthcare, the estimator rapidly returns to the pre-shock baseline, demonstrating resilience. Energy, in contrast, shows a slow but persistent error accumulation, highlighting drift sensitivity. Logistics exhibits incomplete recovery, stabilizing at a higher error floor, while Finance displays long-tail drift with persistent vulnerability. These comparisons reinforce the necessity of domain-specific, drift-aware estimation strategies.

**Table A1** Extended parameter settings for supplementary experimental domains (Logistics and Finance) with drift, shock, noise, regret, sensitivity, and algorithmic details.

Dom.	Category	Value	Description	Drift ( $V_T$ )	Shock	Noise	Regret	Sensitivity	Real-world
1	System size	$n=6$ , $T=250$ , Fleet=300, Depots=3	$k=3$ , 6 routes, 3 vehicle types, – 250 days Transport availability	–	–	–	–	–	–
	Preferences $\theta_t$	$\theta \in \mathbb{R}^6$	Short-haul, Long-haul, +0.01/day (per- Perishable, Express, ishable) Bulk, General	Demand at $t=120$	$\times 2 \sigma^2$ $\{0.01, 0.05, 0.1\}$ and regret	$\in$ Sublinear dynamic	static Drift	$\pm 20\%$ stress test	Fleet Congestion shock
	Cost function	Quadratic delay penalty	$+\ \mathbf{x} - \hat{\theta}\ ^2 + \lambda \cdot \text{delay}$ – $V_T \propto 0.01/\text{day}$	–	–	–	–	–	Airline/trucking scheduling
	Drift schedule	Perishable priority drift	Demand at $t=120$	shock yes	–	Dynamic scaling	regret Drift amplifica- tion	–	Buffering strat- egy
	Noise model	Gaussian	Routing error	observation –	$\mathcal{N}(0, \sigma^2)$	–	Noise scaling	–	Routing resilience scaling Transport data
	Metrics	–	$\ \hat{\theta}_t - \theta_t\ $ , Regret, Delay rate	–	–	–	–	–	Identifiability validation
	Algorithm config	OGD projection	$\Theta = [0, 5]^6$ , step $\eta = -$	–	–	–	–	–	Drift-aware esti- mator
	Initialization	$\hat{\theta}_1 = \mathbf{0}$ , Averaged 20 runs Seeds=42,77,123	–	–	–	–	–	–	Reproducibility
2	System size	$n=5$ , $T=300$	$k=2$ , 5 financial indicators, 2 – constraints, 300 periods	–	–	–	–	–	–
	Capacities	Budget cap, Financial feasibility	–	–	–	–	–	$\pm 10\%$ stress	capital Stress testing
	Regulatory ratios	$\theta \in \mathbb{R}^5$	Profit, Risk, Compliance value, Liquidity, Fair value	Reg. change $\sigma^2$ at $t=150$	$\{0.01, 0.05, 0.1\}$ under noise	$\in$ Sublinear drift	regret drift and $\{0.005, 0.01, 0.02\}$ $\times$ $\sigma^2$	–	Misreporting
	Cost function	Linear + compliance penalty	$c(\mathbf{x}) = \theta^\top \mathbf{x} + -\gamma \cdot \text{compliance cost}$	–	–	–	–	–	Audit and com- pliance
	Drift schedule	$V_T \propto 0.01/\text{day}$	Risk-compliance trade- off drift	Policy shock at $t=150$	–	Dynamic scaling	regret Drift amplifica- tion	–	Market adapta- tion
	Noise model	Gaussian	Reporting noise	–	$\mathcal{N}(0, \sigma^2)$	–	Noise scaling	–	Accounting irregularities
	Metrics	–	$\ \hat{\theta}_t - \theta_t\ $ , Regret, Risk – ratio error	–	–	–	–	–	Performance validation
	Algorithm config	Mirror Descent	$\Theta = [0, 2]^5$ , step $\eta = -$	–	–	–	–	–	Drift-aware esti- mator
	Initialization	$\hat{\theta}_1 = \mathbf{1}$ , Averaged 20 runs Seeds=42,77,123	–	–	–	–	–	–	Reproducibility

<sup>1</sup> Logistics and Transportation domain  
<sup>2</sup> Finance and Accounting domain

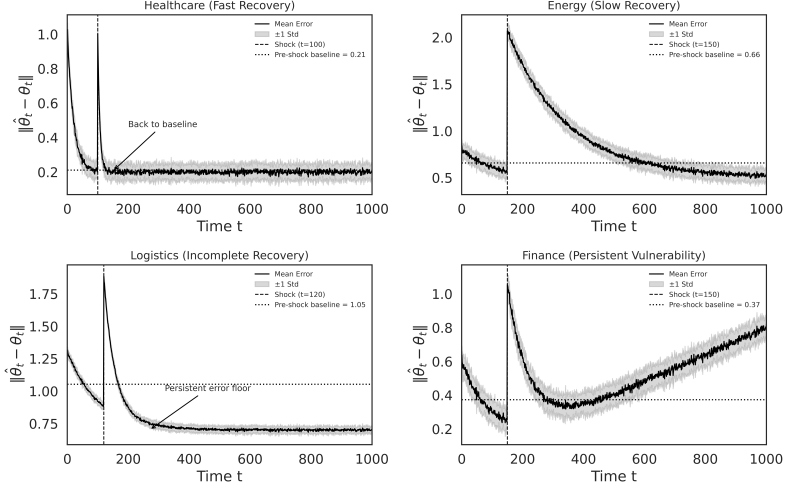


**Fig. A1** Supplementary Figure A1: Recovery error trajectories across four representative domains. Solid black lines denote mean error, gray bands  $\pm 1$  standard deviation, dashed vertical lines mark shock events, and dotted horizontal lines indicate pre-shock baselines.

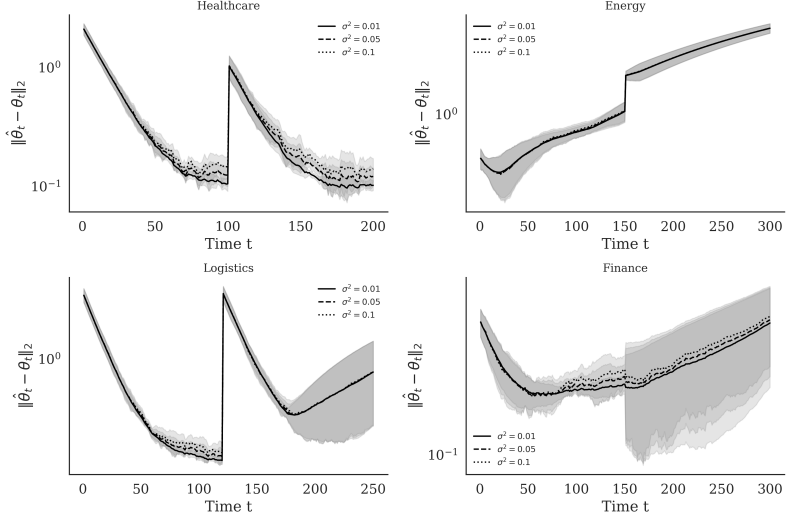


**Fig. A2** Supplementary Figure A3: Noise robustness in the logistics and education domains.

In addition to the healthcare and energy domains reported in Figures 4–5 of the main text, we also examine noise robustness in the logistics and education domains (Supplementary Figure A2). As in the main text, shorter horizons ( $T = 200$  or  $T = 300$ ) are used here to emphasize early sensitivity patterns. This design choice is consistent with Figures 4 and 5, where reduced horizons highlight transient post-shock behavior. Importantly, the horizon length does not alter the qualitative long-run conclusions, but provides a clearer view of early-stage differences across domains.

---

## References

- [1] Ahuja, R.K., Orlin, J.B.: Inverse optimization. *Operations Research* **49**(5), 771–783 (2001) <https://doi.org/10.1287/opre.49.5.771.10606>
- [2] Chan, T.C.Y., Kaw, E., Lee, T.S.: Inverse optimization for the recovery of agent preferences. *Journal of Global Optimization* **59**(2-3), 289–312 (2014) <https://doi.org/10.1007/s10898-013-0091-5>
- [3] Bertsimas, D., Gupta, V., Paschalidis, I.C.: Data-driven inverse optimization. *Mathematical Programming* **153**(2), 595–633 (2015) <https://doi.org/10.1007/s10107-015-0892-2>
- [4] Eshghi, S., Goh, J.: Inverse optimization for the recovery of treatment costs in healthcare. *Operations Research* **64**(6), 1184–1199 (2016) <https://doi.org/10.1287/opre.2016.1546>
- [5] Chan, T.C.Y., Lee, T.S., Terekhov, D.: Inverse optimization: Closed-form solutions, geometry, and goodness of fit. *Management Science* **65**(3), 1115–1135 (2019) <https://doi.org/10.1287/mnsc.2017.2942>
- [6] Besbes, O., Gur, Y., Zeevi, A.: Non-stationary stochastic optimization. *Operations Research* **63**(5), 1227–1244 (2015) <https://doi.org/10.1287/opre.2015.1417>
- [7] Zinkevich, M.: Online convex programming and generalized infinitesimal gradient ascent. In: *Proceedings of the 20th International Conference on Machine Learning (ICML)*, pp. 928–936 (2003). <https://doi.org/10.5555/3041838.3041955>
- [8] Hall, E.C., Willett, R.M.: Online convex optimization in dynamic environments. *IEEE Journal of Selected Topics in Signal Processing* **9**(4), 647–662 (2015) <https://doi.org/10.1109/JSTSP.2015.2416949>
- [9] Sakaue, S., Teraoka, R., Takeda, A.: Online inverse optimization. *Operations Research Letters* **46**(5), 495–500 (2018) <https://doi.org/10.1016/j.orl.2018.07.002>
- [10] Dong, H., Chen, X., Zeng, B.: Generalized inverse optimization through online learning. *Mathematical Programming* **181**(1), 113–148 (2020) <https://doi.org/10.1007/s10107-019-01387-y>
- [11] Ben-Tal, A., Nemirovski, A.: Robust optimization—methodology and applications. *Mathematical Programming* **92**(3), 453–480 (2002) <https://doi.org/10.1007/s101070100286>
- [12] Bertsimas, D., Sim, M.: The price of robustness. *Operations Research* **52**(1),

35–53 (2004) <https://doi.org/10.1287/opre.1030.0065>

[13] Bertsimas, D., Farias, V.F., Trichakis, N.: The price of fairness. *Operations Research* **59**(1), 17–31 (2011) <https://doi.org/10.1287/opre.1100.0865>

[14] Fournier, Z., Leclère, V., Pinson, P.: Fairness by design in shared-energy allocation problems. *Computational Management Science* (2025) <https://doi.org/10.1007/s10287-025-00532-7>

[15] Levi, R., Roundy, R., Shmoys, D.B.: Provably near-optimal sampling-based policies for stochastic inventory control models. *Mathematics of Operations Research* **32**(4), 821–839 (2007) <https://doi.org/10.1287/moor.1070.0274>

[16] Besbes, O., Muharremoglu, A.: Optimal ordering policies with demand learning. *Operations Research* **61**(5), 1104–1118 (2013) <https://doi.org/10.1287/opre.2013.1196>

[17] Westermann, P., *et al.*: Inverse optimal control with time-varying cost functions and its application to human movement analysis. *Scientific Reports* **10**(1), 11732 (2020) <https://doi.org/10.1038/s41598-020-67901-x>

[18] Cao, L., Zhao, H., Wu, J.: Adaptive online inverse optimal control with neural networks. *Biomimetics* **9**(2), 84 (2024) <https://doi.org/10.3390/biomimetics9020084>

[19] Xu, T., Shao, H., Zhang, M.: Inferring commuter preferences for schedule and crowding from aggregate data: An inverse optimization approach. *Transportation Research Part B: Methodological* **177**, 102918 (2024) <https://doi.org/10.1016/j.trb.2024.102918>

[20] Chiang, C.-K., Yang, T., Lee, C.-J., Mahdavi, M., Lu, C.-J., Jin, R.: Online optimization with gradual variations. In: *Conference on Learning Theory (COLT)*, pp. 6–1620 (2012)

[21] Mokhtari, A., Shahrampour, S., Jadbabaie, A., Ribeiro, A.: Online optimization in dynamic environments: Improved regret rates for strongly convex problems. In: *Advances in Neural Information Processing Systems (NeurIPS)*, vol. 29, pp. 2460–2468 (2016)

[22] Zhang, L., Chen, T., Wang, G.: Dynamic regret of strongly convex and smooth functions. In: *Advances in Neural Information Processing Systems (NeurIPS)*, vol. 31, pp. 1082–1092 (2018)

[23] Todorov, E.: Generalized linear models for inverse optimal control. *Neural Computation* **17**(6), 1411–1430 (2005) <https://doi.org/10.1162/0899766053491887>

[24] Abbeel, P., Ng, A.Y.: Apprenticeship learning via inverse reinforcement learning. In: *Proceedings of the 21st International Conference on Machine Learning*

(ICML), pp. 1–8 (2004). <https://doi.org/10.1145/1015330.1015430> . ACM

[25] Ramponi, G., Curi, S., Krause, A.: Truly batch apprenticeship learning with non-stationary rewards. In: Advances in Neural Information Processing Systems (NeurIPS), vol. 33, pp. 19241–19252 (2020)

[26] Bredies, K., Fanzon, S.: Optimal transport regularization of dynamic inverse problems. *ESAIM: Mathematical Modelling and Numerical Analysis* **54**(6), 2089–2119 (2020) <https://doi.org/10.1051/m2an/2020054>

[27] Bredies, K., Carioni, M., Fanzon, S., Romero, M.: A generalized conditional gradient method for dynamic inverse problems. *Foundations of Computational Mathematics* **22**, 1505–1554 (2022) <https://doi.org/10.1007/s10208-021-09523-y>

[28] Bungert, L., Burger, M.: Optimal control and dynamic inverse problems. *Inverse Problems* **37**(10), 104001 (2021) <https://doi.org/10.1088/1361-6420/ac1a4d>

[29] Carioni, M., Schönlieb, C.-B., Song, M.: A generalized conditional gradient method for dynamic inverse problems. *Foundations of Computational Mathematics* (2023) <https://doi.org/10.1007/s10208-023-09588-7>

[30] Polyak, B.T.: Gradient methods for the minimization of functionals. *USSR Comput. Math. Math. Phys.* **3**(4), 864–878 (1963) [https://doi.org/10.1016/0041-5553\(63\)90382-3](https://doi.org/10.1016/0041-5553(63)90382-3)

[31] Łojasiewicz, S.: Une propriété topologique des sous-ensembles analytiques réels. *Les Équations aux Dérivées Partielles*, 87–89 (1963)

[32] Nesterov, Y.: *Introductory Lectures on Convex Optimization: A Basic Course*. Applied Optimization, vol. 87. Springer, Boston, MA (2004). <https://doi.org/10.1007/978-1-4419-8853-9>

[33] Luo, Z.-Q., Tseng, P.: Error bounds and convergence analysis of matrix splitting algorithms for the affine variational inequality problem. *SIAM Journal on Optimization* **2**(1), 43–54 (1992) <https://doi.org/10.1137/0802003>

[34] Bolte, J., Daniilidis, A., Lewis, A., Shapiro, M.: Clarke subgradients of stratifiable functions. *SIAM Journal on Optimization* **18**(2), 556–572 (2007) <https://doi.org/10.1137/060670082>

[35] Bubeck, S.: Convex optimization: Algorithms and complexity. *Foundations and Trends in Machine Learning* **8**(3–4), 231–357 (2015) <https://doi.org/10.1561/2200000050>

[36] Karimi, H., Nutini, J., Schmidt, M.: Linear convergence of gradient and proximal-gradient methods under the polyak–łojasiewicz condition. *Mach. Learn.* **106**(2), 173–206 (2017) <https://doi.org/10.1007/s10994-016-5543-7>

- [37] Hazan, E., Seshadhri, C.: Efficient learning algorithms for changing environments. In: Proceedings of the 26th International Conference on Machine Learning (ICML), pp. 393–400. ACM, ??? (2009). <https://doi.org/10.1145/1553374.1553429>
- [38] Besbes, O., Gur, Y., Zeevi, A.: Non-stationary stochastic optimization. *Operations Research* **63**(5), 1227–1244 (2015) <https://doi.org/10.1287/opre.2015.1391>